

University of Windsor

Scholarship at UWindor

Electronic Theses and Dissertations

Theses, Dissertations, and Major Papers

3-12-2020

Accelerated Testing of Bearings for High Speed Application

Nikunj Rashmikant Patel
University of Windsor

Follow this and additional works at: <https://scholar.uwindsor.ca/etd>

Recommended Citation

Patel, Nikunj Rashmikant, "Accelerated Testing of Bearings for High Speed Application" (2020). *Electronic Theses and Dissertations*. 8326.
<https://scholar.uwindsor.ca/etd/8326>

This online database contains the full-text of PhD dissertations and Masters' theses of University of Windsor students from 1954 forward. These documents are made available for personal study and research purposes only, in accordance with the Canadian Copyright Act and the Creative Commons license—CC BY-NC-ND (Attribution, Non-Commercial, No Derivative Works). Under this license, works must always be attributed to the copyright holder (original author), cannot be used for any commercial purposes, and may not be altered. Any other use would require the permission of the copyright holder. Students may inquire about withdrawing their dissertation and/or thesis from this database. For additional inquiries, please contact the repository administrator via email (scholarship@uwindsor.ca) or by telephone at 519-253-3000ext. 3208.

Accelerated Testing of Bearings for High Speed Application

By

Nikunj Patel

A Thesis
Submitted to the Faculty of Graduate Studies
through the Department of Mechanical, Automotive, and Materials Engineering
in Partial Fulfillment of the Requirements for
the Degree of Master of Applied Science
at the University of Windsor

Windsor, Ontario, Canada

2020

© 2020 Nikunj Patel

Accelerated Testing of Bearings for High Speed Application

by

Nikunj Patel

APPROVED BY:

M. Ahmadi

Department of Electrical and Computer Engineering

B. Minaker

Department of Mechanical, Automotive and Materials Engineering

E. Lang, Co-Advisor

Department of Mechanical, Automotive and Materials Engineering

L. Oriet, Advisor

Department of Mechanical, Automotive and Materials Engineering

February 13, 2020

DECLARATION OF ORIGINALITY

I hereby certify that I am the sole author of this thesis and that no part of this thesis has been published or submitted for publication.

I certify that, to the best of my knowledge, my thesis does not infringe upon anyone's copyright nor violate any proprietary rights and that any ideas, techniques, quotations, or any other material from the work of other people included in my thesis, published or otherwise, are fully acknowledged in accordance with the standard referencing practices. Furthermore, to the extent that I have included copyrighted material that surpasses the bounds of fair dealing within the meaning of the Canadian *Copyright Act*, I certify that I have obtained a written permission from the copyright owner(s) to include such material(s) in my thesis and have included copies of such copyright clearances to my appendix.

I declare that this is a true copy of my thesis, including any final revisions, as approved by my thesis committee and the Graduate Studies office and that this thesis has not been submitted for a higher degree to any other University or Institution.

ABSTRACT

In this research thesis, a new method for accelerated lifetime testing (ALT) of high-speed bearings is discussed. The rapid development of products, and the longer lifespan of bearings on high-speed applications, have generated demand for the accelerated testing method.

A new method is explained for ALT of the bearings. The life of the bearings is reduced by producing higher external force on them. This external force is produced as a result of the gyroscopic couple on a newly developed test bench.

This research paper describes various tests for the validation of the new method of ALT of bearings. Furthermore, experiments are discussed for monitoring the health status of bearings by analysing the electrical current of the Brushless Direct Current motor that is running the bearings in the product.

ACKNOWLEDGEMENTS

This thesis has been made possible thanks to the continuous support of my supervisors and industry partner.

I would like to express my gratitude to Dr. Leo Oriet and Dr. Edward Lang for their continuous support as academic advisors and their shared technical knowledge. Finally, I thank my mom, dad, my friends Sandeep Ghevariya, Dhairya Dhamija and Jainik Shah for their support and motivation in completing my degree. This thesis would not have been feasible without them.

TABLE OF CONTENTS

DECLARATION OF ORIGINALITY	iii
ABSTRACT	iv
ACKNOWLEDGEMENTS	v
LIST OF TABLES	viii
LIST OF FIGURES	ix
LIST OF GRAPHS	x
LIST OF ABBREVIATIONS/SYMBOLS	xi
Chapter 1	1
1.1 Motivation.....	1
1.2 Introduction.....	1
1.3 Objective.....	3
1.4 Thesis Structure.....	4
Chapter 2.....	5
2.1 Literature Review	5
2.2 Limitation of Existing Work	9
2.3 Contribution of This Research	9
Chapter 3.....	11
3.1 Factors Affecting the Bearing Life.....	11
3.2 The Theory Behind the Gyroscopic Couple[18]	12
3.3 Proposed Methodology	14
3.3.1 The Basic Construction of The Bearing Assembly.....	14
3.3.2 Theory	16
3.3.3 Simulation	22

Chapter 4.....	30
4.1 The Purpose Behind Test Bench Development.....	30
4.2 Construction of Developed Test Bench.....	31
4.2.1 Method for Measuring Electrical Current.....	36
4.3 Various Tests on the Test Bench and their Results.....	38
4.3.1 Gyroscopic Couple and Load Measurement by Loadcells.....	38
4.3.2 Trace of Higher Force on the Bearings from Electric Current Measurement...	42
4.3.3 Frequency Domain Representation of the Electrical Signal.....	44
4.4 Tested Pump on Test Bench.....	45
Chapter 5.....	47
5.1 Summary.....	47
5.2 Conclusion.....	47
5.3 Future Work.....	49
5.3.1 Fault Detection of the Bearings.....	49
REFERENCES/BIBLIOGRAPHY.....	57
APPENDICES: A.....	59
MATLAB Code.....	59
APPENDICES: B.....	61
Load Cell Data:.....	61
VITA AUCTORIS.....	62

LIST OF TABLES

Table 1 Expected Life of the Bearings in Various Conditions.....	21
Table 2 Gyroscopic Couple Values Comparison Derived by Simulation and Theory.....	26
Table 3 Theoretical and Simulated Force Comparison on Bearing-1.....	28
Table 4 Theoretical and Simulated Force Comparison on Bearing-2.....	29
Table 5 Readings from Load Cells.....	41
Table 6 Test and Theory Values Comparison.....	42
Table 7 Force Comparison on the Bearings by Various Methods.....	48

LIST OF FIGURES

Figure 1 CAD Image of Components	2
Figure 2 Schematic of Radial and Thrust Bearings[6].....	5
Figure 3 Generation of Gyroscopic Couple[18]	12
Figure 4 Representation of Reactive Gyroscopic couple	13
Figure 5 Example for Understanding the Gyroscopic Couple[18]	14
Figure 6 Exploded View of Ball Bearing[20].....	16
Figure 7 Pump Arrangement for the Generation of Adequate Gyroscopic Force	17
Figure 8 Torque Due to Gyroscopic Couple on Pump Bearing Assembly.....	18
Figure 9 Bearing Mounting Position.....	20
Figure 10 Multibody Dynamic Model for Identifying the Direction of the Gyroscopic Couple	22
Figure 11 Visual Representation of the Simulated Model of Gyroscopic Couple Orientation in MATLAB.....	23
Figure 12 Test Setup Model Representation in the MATLAB-Simulink Environment.....	24
Figure 13 Backbone of the Model of the Test Environment in Simulink	24
Figure 14 Detail View of Impeller Arrangement in the MATLAB Environment	25
Figure 15 Simplified CAD Model for FEA.....	27
Figure 16 Meshing in Simplified Model For FEA.....	27
Figure 17 Boundary Condition Applied to the FEA model.....	28
Figure 18 Developed Test Bench.....	31
Figure 19 Electric Drive Unit for Rotary Table.....	32
Figure 20 Slip Ring Schematic[21].....	33
Figure 21 Testing Table Equipment Schematic Arrangement.....	34
Figure 22 Presence of Noise Because of Sliprings	35
Figure 23 Electrical Current Measurement by Ammeter[22]	36
Figure 24 Electrical Current Measurement by Voltmeter[22]	37
Figure 25 Detail View of Load Cell Test Configuration.....	39
Figure 26 Actual Arrangement of Pump Over the Load Cells	40
Figure 27 Force Acting During Testing	40
Figure 28 Frequency Domain Representation From MATLAB	45

LIST OF GRAPHS

Graph 1 Comparison of Electrical Current Measurement Methods.....	38
Graph 2 Electrical Consumption Comparison During Steady and Rotating Table.....	43
Graph 3 Representation of Measured Electrical Signal in Time Domain	50
Graph 4 Representation of Measured Electrical Signal in Frequency Domain	51
Graph 5 Fault Detection from Time Domain Electrical Signal	52
Graph 6 Fault Detection from Frequency Domain Electrical Signal	52
Graph 7 Generated IMF from the EMD of Pump-2.....	54
Graph 8 Scatter Plot of Healthy and Faulty Bearings	55

LIST OF ABBREVIATIONS/SYMBOLS

RPM	Revolution Per Minute
C	Gyroscopic couple
ω	Angular velocity
FEA	Finite Element Analysis
CAD	Computer Aided Design
DAQ	Data Acquisition Unit
A	Ampere
V	Volt
DC	Direct Current
FFT	Fast Fourier Transform
ms	Millisecond
kHz	Kilohertz
EMD	Empirical Mode Decomposition
IMF	Intrinsic Mode Functions
CBM	Conditional Based Monitoring
FDD	Fault Detection and Diagnosis
ALT	Accelerated Lifetime Testing
BPI	Ball Pass Frequency of Inner Ring
BPFO	Ball Pass Frequency of Outer Ring
SMPS	Switched Mode Power Supply
CG	Center of Gravity
BLDC	Brush Less Direct Current
Ω	Ohm

Chapter 1

Introduction

1.1 Motivation

A bearing is a machine element that helps in achieving the relative motion between two bodies or elements[1]. The main function of the bearing is to reduce friction between two objects, that are in mechanical contact and in relative motion with each other. Based on the various applications and requirements, many types of bearings are available on the market. Applications of bearings range from the deep sea to space and from kitchens to sophisticated nuclear powerhouses[2]. Due to advancements in metallurgy and tribology, new bearings can withstand millions of revolutions and harsh working conditions[3]. Any unpredicted bearing failure in a wind-turbine, jet-engine or a Nuclear plant may cause high maintenance costs and downtime[4].

Bearings are selected during the initial development stage of a product based on theoretical calculations and the projected life of a product. The life of bearings is dependent upon many parameters[5], and consequently, it is hard to estimate the life of bearings in respective working conditions. Due to the critical applications of bearings, however, it is crucial to have an idea as to their expected lifespan. Therefore, bearings need to be tested for failure predictions and life expectancy.

During the development phase, testing time might be longer in the case of bearings with greater longevity. The longer life of the bearings leads to further delay in product development and results in a final product with higher costs. To eliminate long testing time, some accelerated testing methodologies are developed to test such bearings. Accelerated lifetime testing (ALT) is one of the processes employed to speed up the degradation of a component by overloading it to uncover faults in a short amount of time[3].

1.2 Introduction

In this research, a new method of ALT of the bearings is discussed. This newly developed method is concentrated on the specific application and is limited due to some pre-defined application constraints. The objective behind this research is to develop a new method for accelerated lifetime testing of the bearings and provide ample information for validation. The long-term research goal is to monitor the health of the bearings by analyzing the electrical current from the Brush Less Direct Current (BLDC) motor that drives the bearings.

This research helps to reduce the overall product development time by introducing a new method of ALT of the bearing.

In the newly developed method, a test bench is developed that creates conditions to produce the gyroscopic couple. This developed gyroscopic couple generates a higher force on the bearings, which in turn leads to accelerated bearing wear. Because of a higher rate of wear, the bearings face earlier failure as compared to the projected life of the bearings in ideal conditions. Use of a gyroscopic couple to accelerate the wear of the bearings is a new method for ALT of the bearing.

Before proceeding in further detail, some brief information about the selected products is discussed in this section, in order to provide an overview of the product and arrangement of bearings in the final application.

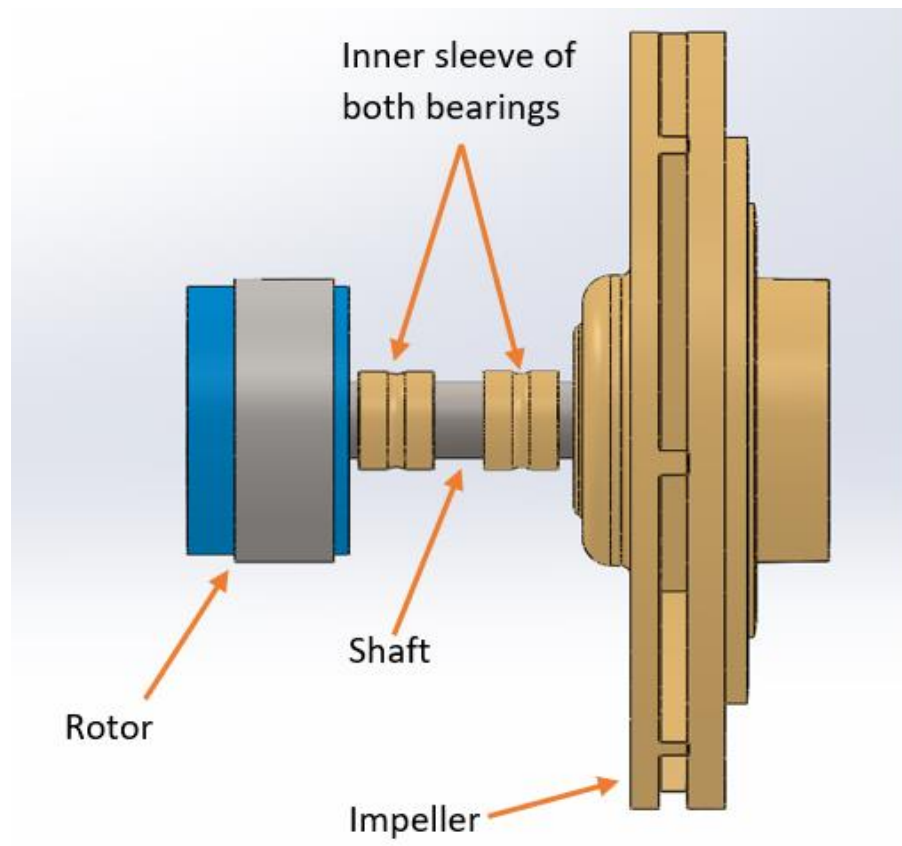


Figure 1 CAD Image of Components[6]

In this research an ALT of the bearings is carried out while bearings are assembled in the final product. The final product is a pump that is used to transfer gaseous fluid.

The primary components of the pump body are an impeller, a shaft, two bearings, a BLDC motor, and a controller of the BLDC motor. The BLDC motor includes a permanent magnetic rotor and a three-pole stator. The cartridge is made from the assembly of the bearings. A shaft is inserted through this bearing assembly and the whole assembly is inserted into the casing of the pump. One end of the shaft supports the impeller and another end of the shaft supports a permanent magnetic rotor. The permanent magnetic rotor is a part of the BLDC motor.

For further illustration, refer the Figure 1, which represents the computer aided design (CAD) model of the components. The image of the final product is not displayed due to the confidentiality agreement with the industry partner. In Figure 1, note that the function of the bearing is to support the shaft, including the impeller and the permanent magnetic rotor. Here, instead of the whole bearing assembly, only the inner sleeves of the bearings are shown.

The bearings described are deep groove ball bearings. They are selected based on the projected life of 8000 hours. Both bearings are sealed from both sides. They are pre-lubricated and do not require any lubrication during the whole working life. The purpose of bearing seals is to protect both bearings from external contamination.

The permanent magnetic rotor is surrounded by the stator of the BLDC motor. The required torque and angular velocity are transferred to the impeller with the help of the shaft due to the magnetic interference between stator and rotor. Because of this construction, two bearings provide support to all rotating components. The impeller creates the pressure difference to deliver an adequate flow of gaseous fluid. The BLDC motor requires a controller in order to function, and this controller is included inside the body of the pump.

1.3 Objective

The objectives are divided into two groups. The first targets the ALT of the bearings. The second concentrates on the detection of faults in the bearings by analyzing the electrical current of the BLDC motor.

Objectives related to the first group are herein, whereas the latter is briefly touched upon with avenues for potential future research.

Few initial studies have been carried out related to the second group of objectives. Therefore, future research will provide a basis from which to build on fault detection of the bearings. These objectives are defined by considering the requirements of the industry partner.

- Identify the most suitable method for ALT of the bearings based on the selected application and constraints;
- Validate the newly proposed method based on the theory and simulated data;
- Setup a test bench for validating the theoretical method and be capable of collecting high-resolution electrical traces from the BLDC motor of the pump; and
- Identify the bearing wear or fault detection in the bearings by measuring the electrical current of the motor that drives the pump installed with the bearings.

1.4 Thesis Structure

Chapter 2 introduces two of the key existing methods of ALT of bearings. The advantages and limitations of these existing methods are discussed. This chapter also covers the requirement of the new method compared to traditional methods.

The third chapter describes the newly developed method of ALT of bearings in detail. The theory behind the new method is elaborated and the theory is supported by simulations. Justification is given as to how the new method is unique and best suited for the defined criteria with few constraints.

The development and construction of the new test bench is demonstrated in Chapter 4, with an explanation of the utility of the new test setup for ALT of the bearings. The data acquisition method from the electrical motor is also discussed. This represents a validation of a new method by demonstrating various practical and theoretical proofs from different analyses and tests. Moreover, several methods of fault detection of the bearings are described.

The final chapter concludes the thesis by summarizing major findings and proposes ideas for future research.

Chapter 2 Background

2.1 Literature Review

As mentioned previously, a bearing is a machine element that provides support to another machine element. It permits a relative motion between the contact surfaces of the members, while carrying the load[1]. Bearings are an important part of industrial equipment as their components are subjected to harsh operating environments and hence experience significant wear and tear[2].

Bearings are classified into two categories[1], according to the direction of load to be supported or the nature of contact between surfaces.

- Based on the direction of the load to be support
 - I. Radial bearing: the load acts perpendicular to the direction of the moving element.
 - II. Thrust bearing: the load acts along the axis of rotation.

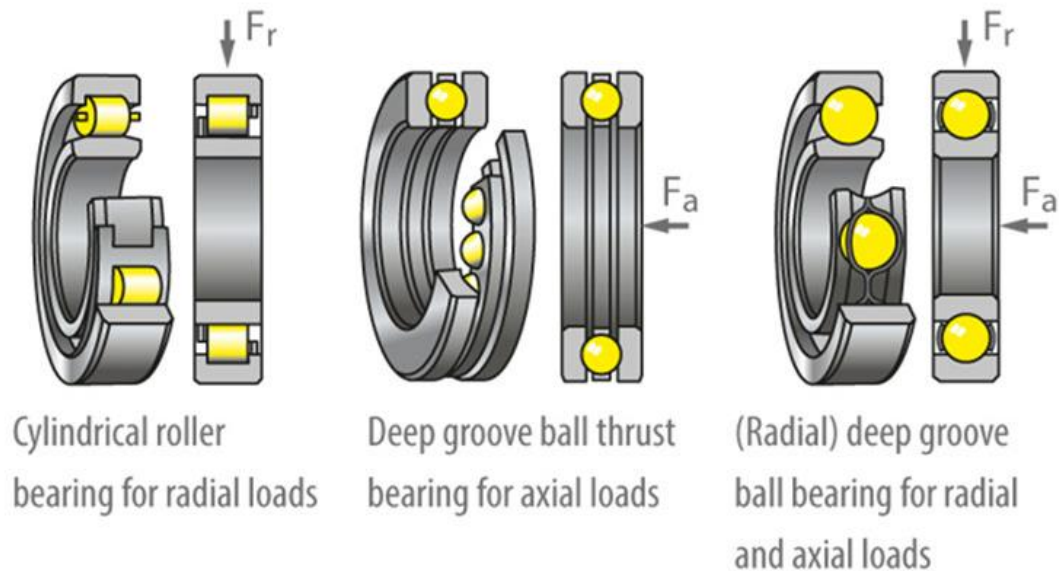


Figure 2 Schematic of Radial and Thrust Bearings[7]

- Based on the nature of the contact
 - I. Sliding contact bearing: the sliding takes place along the surfaces of contact between the moving element and the fixed element.
 - II. Rolling contact bearing: the steel balls or rollers are interposed between the moving and fixed elements. The balls offer rolling friction at two points for each ball or roller.

Only rolling contact bearings with radial load are discussed for this study. Radial deep groove ball bearings are used to conduct this thesis work.

As discussed, bearings have many critical applications. Because of their critical applications, it is necessary to test bearings within adequate parameters in order to validate their performance.

Bearing life depends on many parameters, such as applied equivalent load, temperature, type of load (continuous load, fatigue load, and impact load), lubrication, exposure to the environment (working conditions), and/or contamination within lubricant[3][8]. Bearing wear can be accelerated by varying any of these parameters, and consequently causing the bearing to fail before the expected life in standard conditions.

The most popular method for ALT of bearings is providing an external excessive force on bearings in a controlled manner[3]. Bearing life is defined by the applied load during working conditions and the number of revolutions that bearing endures[9]. Because the force is higher than the load rating, the bearing wears more quickly and gradually fails before its rated life.

$$L_{10} = \left(\frac{C}{F}\right)^p \quad \text{Equation 1}$$

Where,

L_{10} = bearing life, the point at which 10% of the bearing will fail

C = basic dynamic load rating of the bearings

F = applied load

p = a power: 3 for ball bearing, 10/3 for the typical roller

Equation 1 represents the expected life rating of the bearing[3][9]. The bearing life " L_{10} " is inversely related to "p" the power of the applied force "F". The higher the force, the lesser the life of the bearing. In other words, a higher force accelerates the mechanical wear of the bearings, and bearings fail earlier due to the higher rate of wear. In author[3], higher axial and radial force are applied in a controlled manner to accelerate the wear of the bearings, and two electrical actuators are used to apply the external force.

In research paper[10], the elevated temperature is selected as the cause of the rapid wear of the bearings. As per the paper, temperature influences the life of the bearings more than any other factors.

The state of the lubricant is extremely important in order to achieve an optimum life of the bearings. An elevated temperature is still the greatest enemy of the lubricant, because the lubrication oil and grease cannot withstand higher temperatures, which cause them to begin to degrade. Therefore, elevated temperature becomes a primary cause for the shorter life of the bearings[11]. These types of scenarios create bearing defects such as cracking, pitting, and metal contamination in the lubricant. The Arrhenius model considers the temperature effect on the life of the bearing; however, there is not a detailed method for the implementation of the Arrhenius model on the rolling bearings[12][10].

Bearing wear is accelerated in[13] through electrical stress. An adequate amount of electrical current is passed in order to apply the electrical stress to the bearing. This stress leads to pitting on the bearing sleeve and creates the mechanical damage on the bearings. As a result, accelerating bearing wear from electrical stress is another option for ALT of bearings.

The primary use of fault detection is in maintenance. There are three types of methods in the maintenance[14][15].

1. Run to Break Maintenance: the machine is run until the failure of any component occurs and the machine comes to a breakdown condition. This type of maintenance is preferred on small-scale machines and used less frequently for larger machines.
2. Time Based Preventive Maintenance: for a specific machine, a time interval is defined for repair. The meantime to repair is less than the meantime to failure. During the repair time, various parts of a machine are inspected for possible types of wear or any trace of failure.
3. Condition Based Maintenance: currently, this is the most widely used method for complex machines. During normal function, the machine is continuously observed on various parameters. Whether the machine is functioning appropriately or not is defined by analyzing these parameters. There are many techniques that are established for Fault Detection and Diagnosis (FDD).

In paper[3], the fault detection method from the vibration signal is discussed. In this method, a vibration signal is measured from an accelerometer, which is mounted on the bearing assembly. An accelerometer measures the vibration produced from the bearings. This vibration is a signature of

the mechanical defects during testing. That specific frequency and energy of the signal can be extracted from the frequency domain representation of the measured signal.

A worn bearing has a higher friction, which increases the machine temperature, noise, and vibration levels. A completely worn bearing could cause total system failure, injuries, and costly downtime. The cause of the vibration in the bearings is a fault in an inner racer, outer racer or the pitting on various parts of the bearings[4]. Two key methods for monitoring the health of the bearings are vibration and lubrication analysis[2][4]. Vibration analysis performs efficiently because a minor fault in the machine creates no change in its chemical composition, but does increase the intensity of vibration and is easy to detect[16].

When there is any defect, a bearing creates vibration during rotation. Because of the rotation of the bearing at a specific angular speed, a bearing creates a periodic event of the vibration that creates the frequency. Therefore, vibration analysis is very similar to frequency analysis. The method or algorithm used to analyze the normal signal can be utilized to analyze the signal from faulty bearings[16].

The Ball Pass Frequency of Inner Ring (BPFI) and Ball Pass Frequency of Outer Ring (BPFO) can be calculated based on the construction of the bearing and revolution speed. From them, fault location can be identified, whether a fault is in the outer racer or the inner racer[4].

Vibration signal can be categorized based upon their domain of measurement[17]:

1. Time domain
2. Frequency domain
3. Time-Frequency domain

Root Mean Square (RMS), Kurtosis, Crest Factor and Standard Deviation parameters are some examples of time domain metrics.

In author[4], in addition to the fault detection of the bearing from the vibration signal, fault detection of the BLDC motor is presented from the measurement of electrical current from the poles of the stator.

2.2 Limitation of Existing Work

In Section 2, two major topics are covered. The first is various methods of ALT of bearings and the second is failure detection of bearing by analyzing the vibration signature from the bearings. Here, the limitations of the existing method are discussed.

As outlined in[3], a special arrangement is required to apply an external force on the bearings. Bearings are not assembled in the application. Therefore, it is not possible to test the bearings after the assembly. Some bearings are preloaded before the assembly and some after the assembly. These arrangements of bearings cannot be tested in the accordance to the method outlined using the test bench in[3].

As described in[10], the accelerated lifetime test of bearings is possible by increasing the temperature. However, the suggested Arrhenius model is limited to applications involving rolling bearings.

For condition monitoring of bearings, the vibration signature is widely acknowledged as a reliable gauge of the bearings' health status[3]. Different types and locations of the faults can be detected by analyzing the bearing vibration. An accelerometer is required with the proper configurations to collect vibrations from the bearings. Sometimes, setting up an accelerometer on the bearings is a costly testing setup.

2.3 Contribution of This Research

In this research, a novel method is discussed on ALT of the bearings. This newly developed method can apply a higher external force on the bearings by generating a gyroscopic couple.

This unique method is suitable for the high-speed radial ball-bearings life test. The method proposed here is to utilize radial force induced by a gyroscopic couple of rotating parts. In selected applications, bearings are assembled into a pump, and the function of the pump is to transfer gaseous fluid. The impeller, shaft, and rotor of the motor are supported by two deep groove ball bearings mounted inside the casing of the pump. The impeller speed of the pump is 60,000 RPM, these high-speed spinning components help to establish adequate gyroscopic couple on the bearings. In other words, these high-speed spinning components enable the bearings to be tested with this method.

A special test bench is developed to verify this research and theory. This test bench is built in such a way that it can create a gyroscopic couple in a controlled manner and this gyroscopic couple becomes the source of the radial force on the bearing. This radial force accelerates the bearing wear, which helps to reduce the life of both deep groove ball bearings. Because of this innovative concept, it is possible to do an ALT of the bearings while bearings are assembled in the product. This test arrangement is nearer to the final application of the bearings in the product compared to the testing of the bearings individually.

In addition to accelerated testing of the bearings, two tests are discussed on the fault detection of the bearings. In these fault detection methods, fault of the bearings is detected by analyzing electrical current of the BLDC motor instead of the vibration signal of the bearings. This will provide the initial basis for future research. With these methods, two pumps are distinguished in a graph for the pump with faulty bearings and the pump with healthy bearings.

Chapter 3 Theory and Methodology

3.1 Factors Affecting the Bearing Life

The life of the bearing depends on many factors. Below are some factors on which bearing life depend.

Factors affecting bearing life[18]:

- I. Ambient or working temperature
- II. The mean speed of the bearing
- III. The Nature of loading conditions on the bearing
- IV. Lubrication and Contamination
- V. Assembly condition and preloading

Although it is hard to represent bearing life in a small formula, for simplicity it can be represented in equation form[9]

$$L_{10} = \left(\frac{C}{F}\right)^p \quad \text{Equation 1}$$

Where,

L_{10} = bearing life, the point at which 10% of the bearings will fail

C = basic dynamic load rating of the bearings

F = applied load

p = a power: 3 for ball bearing, 4 for pure line contact bearing, 10/3 for the typical roller bearing.

By varying the above parameters, it is possible to change the expected useful life of the bearings. Many accelerated testing methods already exist based on the higher ambient temperature. Elevated temperature directly affects the lubrication property and leads to increased bearing wear. Another factor is the mean speed. Bearing wear can be increased by raising the mean speed of the bearings. Similarly, higher load also accelerates the bearing wear. Thus, higher load, temperature and speed of the bearings are the major factors affecting the bearing life. Controlling these factors plays a major role in ALT of the bearings.

3.2 The Theory Behind the Gyroscopic Couple[19]

In this segment, a brief overview of the Gyroscopic effect is described.

Consider a disc is spinning with angular velocity ω rad/s about the axis OX , in a counterclockwise direction when seen from the front, as shown in Figure 3. Since the plane in which the disc is rotating is parallel to the plane YOZ , it is called the plane of spinning. The plane XOZ is a horizontal plane, and the axis of spin rotates in a plane parallel to the horizontal plane about an axis OY . In other words, the axis of spin is said to be rotating or precessing about an axis OY (which is perpendicular to both the axes OX and OZ) at an angular velocity ω_p rad/s. This horizontal plane XOZ is called the plane of precession and OY is the axis of precession.

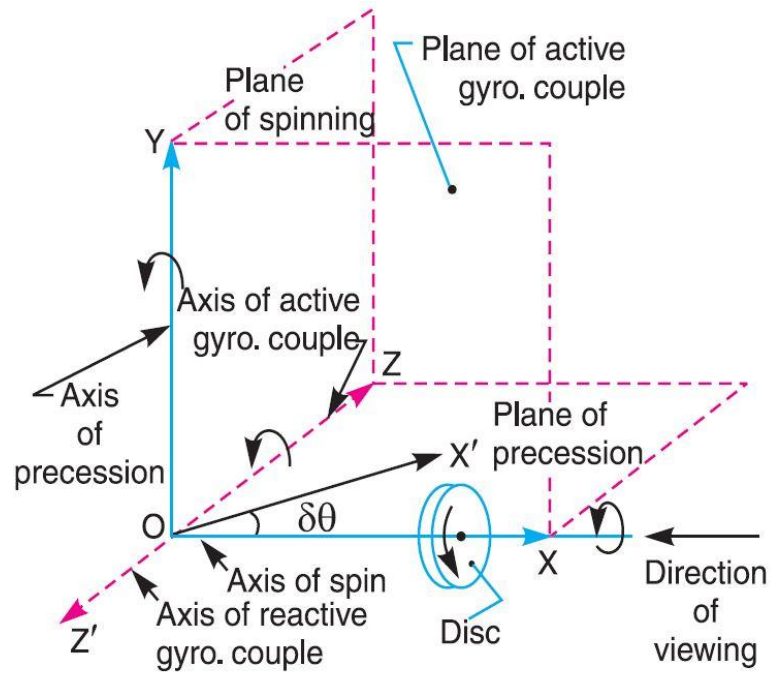


Figure 3 Generation of Gyroscopic Couple[19]

Let, $I =$ Mass moment of inertia of the disc about OX , and

$\omega =$ Angular velocity of the disc

angular momentum of the disc can be found:

$$= I \cdot \omega$$

Angular momentum is a vector quantity, due to the fact that it can be represented by vector $\vec{Ox'}$, as shown in Figure 4.

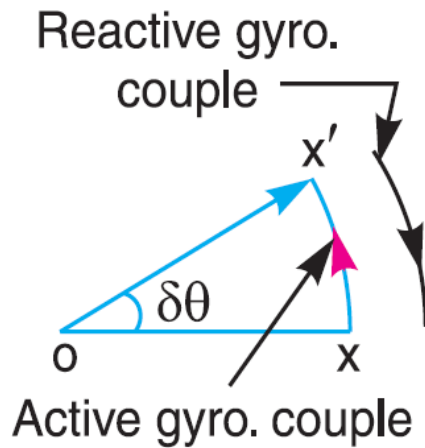


Figure 4 Representation of Reactive Gyroscopic couple

Change into angular momentum

$$= \overrightarrow{OX'} - \overrightarrow{OX} = \overrightarrow{XX'} = \overrightarrow{OX} \cdot \delta\theta$$

$$= I \cdot \omega \cdot \delta\theta$$

And the rate of change of angular momentum

$$= I \cdot \omega \times \frac{\delta\theta}{dt}$$

Since the rate of change of angular momentum will result by the application of a couple to the disc, therefore the couple applied to the disc causing precession is,

$$C = \lim_{\delta t \rightarrow 0} I \cdot \omega \times \frac{d\theta}{dt}$$

$$= I \cdot \omega \cdot \omega_p \dots\dots\dots (1)$$

This is the theoretical representation of the effect and value of gyroscopic couples. Due to the active gyroscopic couple disc trying to rotate in such a way that angular velocity can be represented by $\overrightarrow{OZ'}$. As the gyroscopic couple is a vector quantity, the direction of the gyroscopic couple can be changed by varying the direction of any one input velocity, by changing either the spinning direction of the impeller or altering the turn of the airplane, as shown in the example provided below in Figure 5:

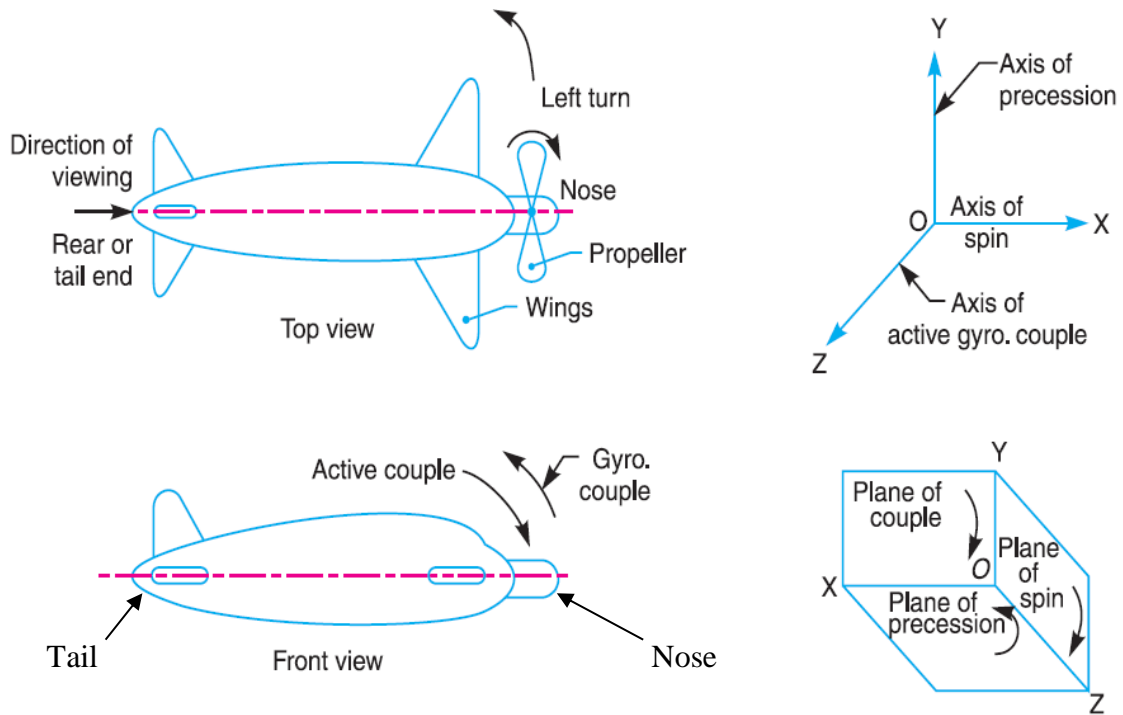


Figure 5 Example for Understanding the Gyroscopic Couple[19]

Here, the gyroscopic effect occurs for an airplane in defined conditions. Let us assume in the example provided, that the propeller rotates in the clockwise direction when seen from the rear tail, and that the airplane takes a left turn when seen from the top view, as illustrated in the top view in Figure 5. Here, the gyroscopic couple reacts in such a way that it raises the nose and lower the tail.

In another case, if the airplane takes a right turn, then the gyroscopic couple acts in such a way that it lowers the nose and raises the tail. These two examples will be useful in understanding the theory behind this research paper.

3.3 Proposed Methodology

In this section, the method of how radial force is generated by the gyroscopic couple and how the radial force accelerates wear of the bearings is described. This theory is supported by simulation data.

3.3.1 The Basic Construction of The Bearing Assembly

From Figure 1, the basic arrangement of the bearings and other components can be seen. Due to the confidentiality of the product, some information about the product is withheld.

Figure 1 illustrates the relevant arrangement of the inner sleeves of the bearings, a shaft, and the permanent magnetic rotor of the motor and the impeller. Both bearings support all of the spinning components inside the casing of the pump. One shaft is inserted through both of the bearings. The permanent magnetic rotor of the BLDC motor is mounted at one end of the shaft. The impeller is mounted on another end of the shaft. The function of the shaft is to transfer the required torque and motion to the impeller, and as a result, the impeller can create an adequate pressure difference to generate the required flow of the gaseous fluid.

In Figure 1, only the inner sleeves of the bearings are shown, instead of the entire bearings. For this research, the selected bearings are deep groove radial ball bearings. The basic construction of similar ball bearings can be understood in Figure 6. It has several balls, which are fitted between inner and outer sleeves (also called inner or outer rings). All balls are separated with the help of the retainer.

Another function of the retainer is to prevent ball to ball contact, in order to reduce the chance of metal to metal contact among the balls. Such use of the retainer increases the life of the bearings[20]. The function of the balls is to create rolling friction between the inner and the outer rings. Proper grooves inside both rings provide precise motion between both rings (inner and outer rings). Thus, the function of the bearing is not only to provide less friction but also to deliver a precise location.

Both ends of the bearings are covered with the shields. The function of the shield is to prevent direct contact of the inner parts, such as the balls and retainers from the external atmosphere and to reduce the chance of contamination of the lubricant. Shields are placed and fixed properly with the help of the circlips.

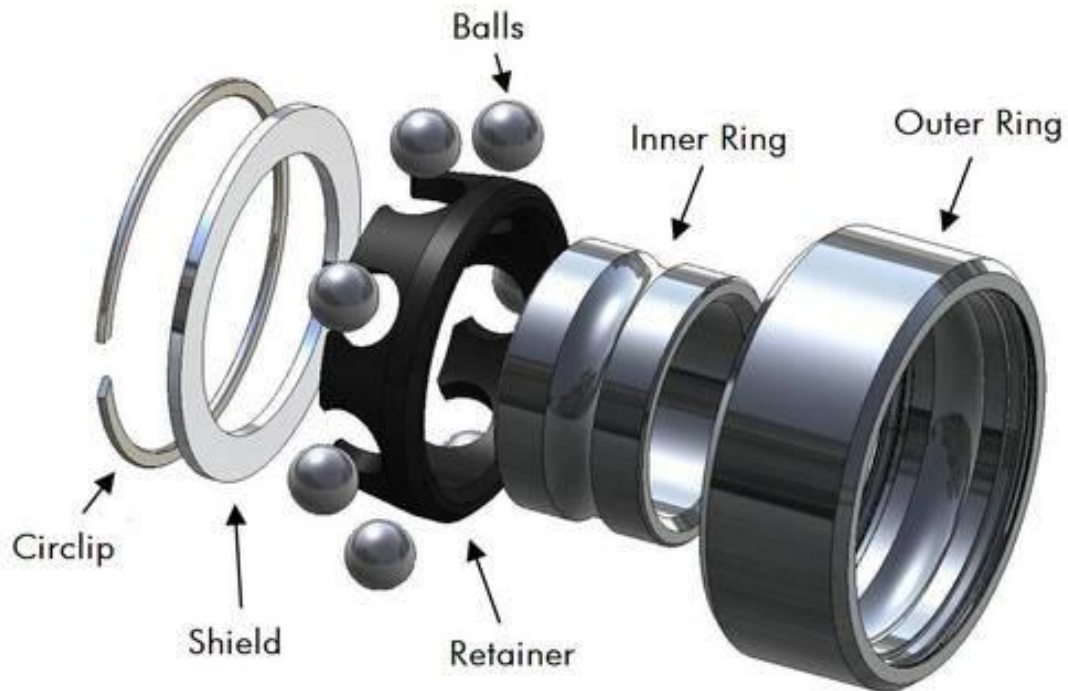


Figure 6 Exploded View of Ball Bearing[21]

3.3.2 Theory

In this section, the theory behind the generation of the gyroscopic couple and transformation of it as a radial force on bearings is explained.

To generate a gyroscopic couple, the bearings and the impeller assembly is arranged as shown in Figure 7. The axis of rotation of the impeller should be parallel with the plane of the table and perpendicular to the axis of rotation of the table. The table is rotating with respect to the vertical axis and in clockwise direction when seen from the top view. The impeller is rotating along the horizontal axis. On account of the confidentiality of the product, only important internal components are illustrated in Figure 7. These components are responsible for the generation of the gyroscopic couple.

As noted in Figure 5, the pump shares similarities in generating a gyroscopic couple with the example of the airplane. Instead of the impeller of the airplane, here it is the impeller of the pump. When the plane makes a left turn, the mounted pump on the table makes right revolutions. Because of the gyroscopic couple, the plane tilts down at its backside. The spinning components (shaft, impeller and rotor) are trying to tilt the shaft, as shown in Figure 8.

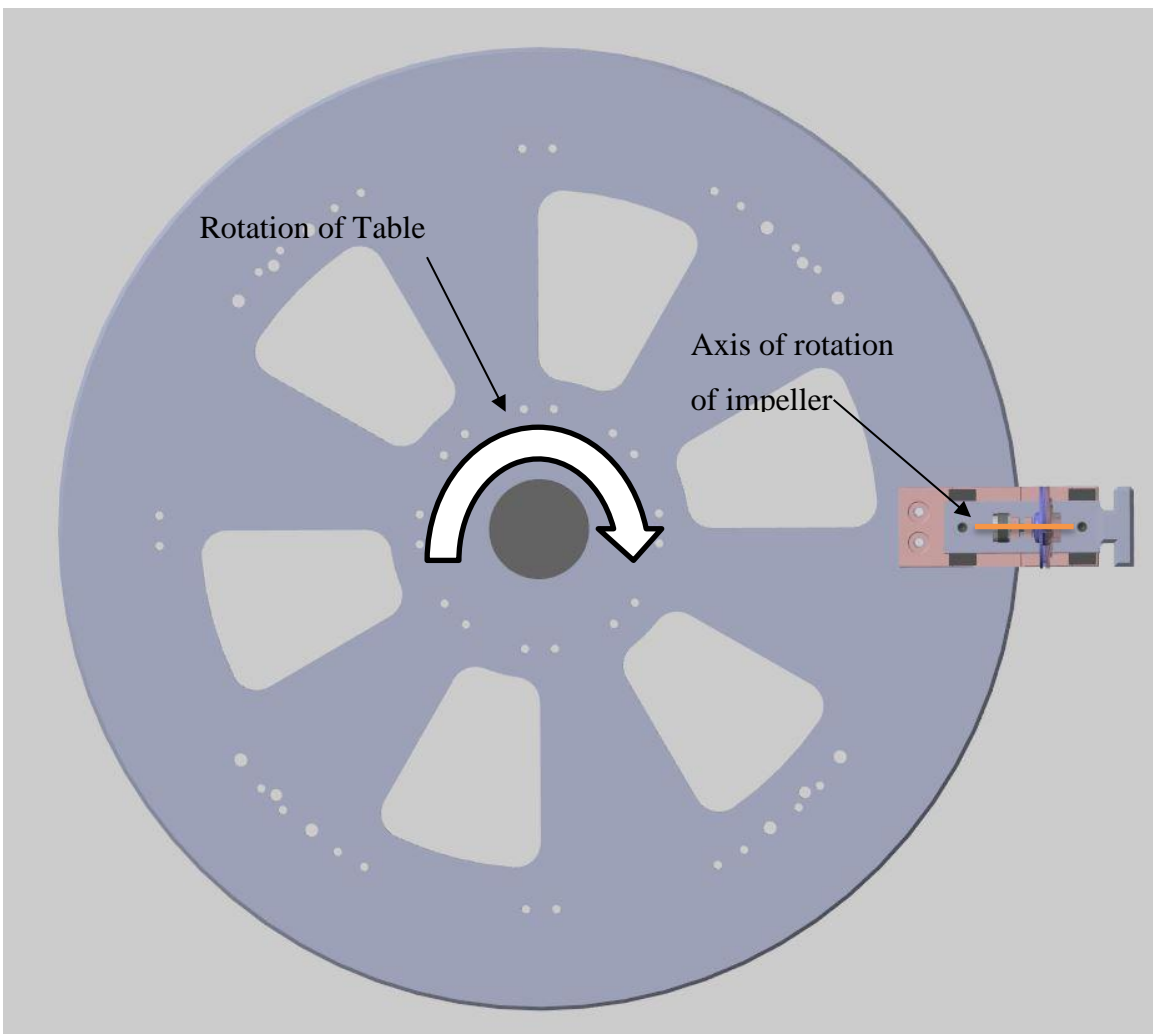
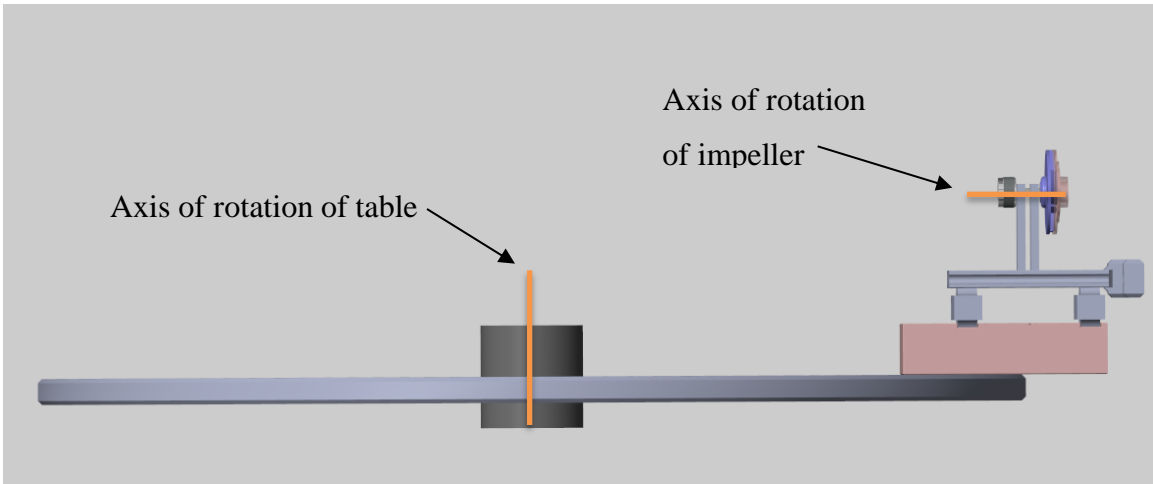


Figure 7 Pump Arrangement for the Generation of Adequate Gyroscopic Force

Because of the mounting of the bearings, it is not possible to tilt the shaft, and the reaction force from the casing of the pump is applied on both bearings to keep the shaft in the horizontal position.

These radial forces on both of the bearings are nearly equal in amplitude but opposite in directions. Eventually, this force causes the expedited wear of the bearing. This rapid wear in turn reduces the bearing testing time.

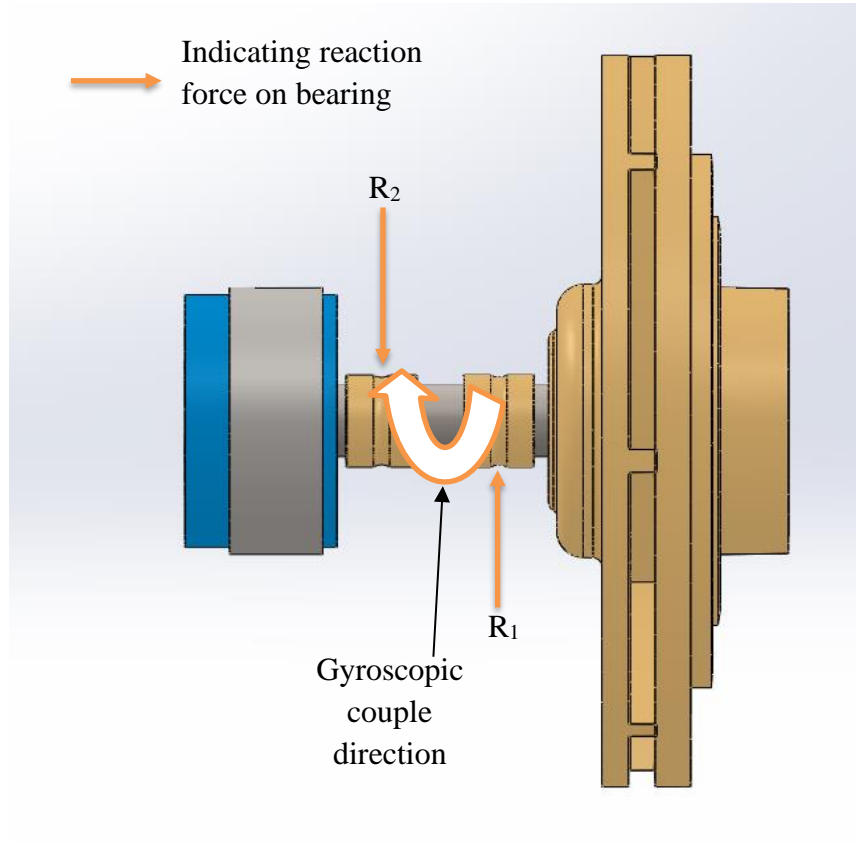


Figure 8 Torque Due to Gyroscopic Couple on Pump Bearing Assembly

Figure 8 illustrates the direction of the gyroscopic couple in the aforementioned example. In this illustrated view, rotation is in the clockwise direction. The orientation of the gyroscopic couple can be changed by varying the direction of the spinning table, as shown in Figure 7 (it is clockwise).

As per section 3.2, the moment of inertia is required to calculate the gyroscopic couple. Force acting on the bearings is calculated from the derived value of the gyroscopic couple.

3.3.2.1 Deriving the Value of the Produced Gyroscopic Couple

From section 3.2, the value of the gyroscopic couple is

$$C = I \cdot \omega \cdot \omega_p$$

The impeller is rotating at 60,000 RPM and the table on which the pump is mounted is rotating at 200 RPM.

Therefore, the angular velocity of the impeller $\omega = 6283.2 \text{ rad/s}$

Angular velocity of the table $\omega_p = 21.26 \text{ rad/s}$

The theoretical calculation for the moment of inertia is complicated because of the shape of the impeller and the complex internal construction of the permanent magnet rotor. Therefore, a commercial 3D CAD platform is used to calculate the moment of inertia of the spinning components.

Moment of inertia of spinning components is $I = 1.6\text{E-}06 \text{ kg.m}^2$.

$$\text{As, } C = I \cdot \omega \cdot \omega_p$$

Therefore, the gyroscopic couple is $C = 0.21 \text{ Nm}$

3.3.2.2 Force Acting on the Bearing Due to the Gyroscopic Couple

In the previous section, the value of the gyroscopic couple was calculated. In this section, force on the bearings is derived from the gyroscopic couple.

From Figure 9, it is noted that two bearings are mounted on the shaft with a distance of “a”. Distance from the center of the shaft for each bearing is “b” and “c” respectively. Their values are as follows:

$$a = 6.6 \text{ mm}; b = 3.182 \text{ mm}; c = 3.418 \text{ mm}$$

These values are important for the calculation of the force acting on each bearing from the gyroscopic couple.

Forces are resolved by considering that the gyroscopic couple is acting clockwise in Figure 8 and bearing-2 is fixed. Then the reaction force on the bearing-1 is

$$\begin{aligned} R_1 &= (C + m g b)/a \\ &= 31.91 \text{ N} \end{aligned}$$

The force acting on the bearing-2 is

$$R_2 = (C - m g c)/a$$

$$= 31.72 \text{ N}$$

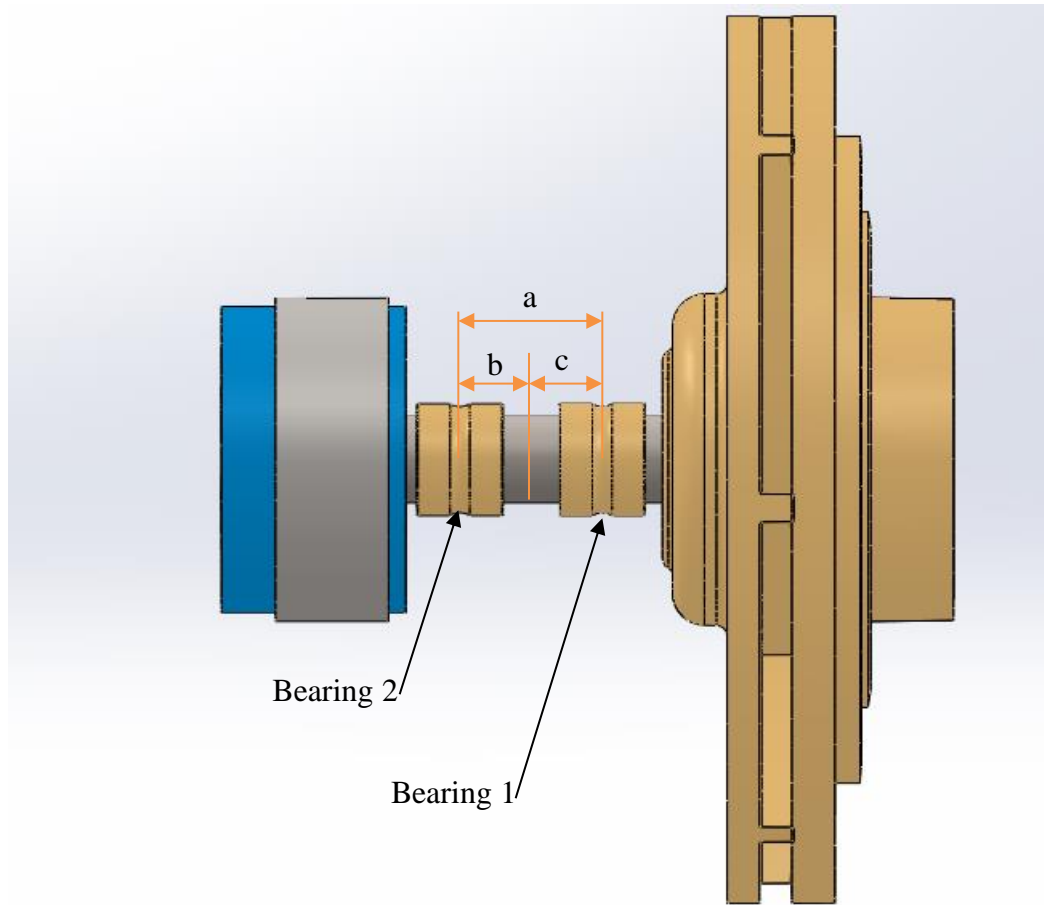


Figure 9 Bearing Mounting Position

In this way, the force on both bearings is calculated based on the law of conservation of force in the system. Based on the selected spinning direction of the impeller and the table, the gyroscopic couple acts in clockwise direction. In the opposite situation, the forces acting on the bearings can be calculated with the same method, and the values of force on the bearings would be similar.

3.3.2.3 Predicted Life of the Bearing in Defined Conditions

Theoretically, force acting on the bearings is acquired. Force, pump RPM, and temperature are the known parameters of the bearings in this application. The expected life of the bearings can be calculated by considering these parameters as per section 3.1. Moreover, loading pattern and assembly condition of the bearings are useful to calculate the life of the bearings.

However, bearing suppliers have more complicated internally developed tools for calculating the life of the bearings. Therefore, for this research, support from the bearing manufacturer was received and considered in order to estimate the life of the bearings during a specific testing method.

Under the normal working conditions, the expected life of the bearings studied is approximately 8000 hours. However, the aim of ALT is to compress the testing time to less than 8000 hours. In this current thesis, the target set to compress the testing time is approximately 350 hours.

Joint work carried out with a bearing manufacturer concluded that a force of 32 N should be applied on each bearing to reduce the life of the bearing to 350 hours. A summary of cases is presented in Table 1.

Table 1 Expected Life of the Bearings in Various Conditions

	Case 1	Case 2	Case 3	Case 4
Impeller Speed (RPM)	50,000	60,000	60,000	60,000
Table Speed (RPM)	100	90	200	230
Temp (°C)	100	100	100	100
Produced radial load on bearing-1 (N)	13.2	14.26	31.8	36.59
Produced radial load on bearing-2 (N)	13.3	14.45	31.99	36.77
Axial load (N)	0.26	0.21	1	1.4
Bearing-1 life (hours)	N/A	4661	316	227
Bearing-2 life (hours)	N/A	3900	381	278

Considering the data from Table 1, 32 N force should be applied to the bearing to compress the life of the bearings to approximately 350 hours. Therefore, the speed of the spinning table should be set in such a way that it can generate an adequate gyroscopic couple to lead to building 32 N on the bearings. In other words, in order to achieve 32 N of force on the bearings, the spinning speed of the table should be set to 200 RPM.

Therefore, considering theories from section 3.3.2.2 and 3.3.2.1, if the table speed is set to 200 RPM, then the value of the produced gyroscopic couple is capable of generating approximately 32 N on each bearing, and the life of the bearing is compressed to around 350 hours.

3.3.3 Simulation

Simulations have been carried out for verification of theoretical calculations. Below is the description of these simulations.

3.3.3.1 Simulation for the Gyroscopic Couple Generation

Two models are developed in the MATLAB-Simulink environment. One model is developed to verify the generation of the gyroscopic couple. The simulation model also verifies the direction of the gyroscopic couple depending on the direction of rotation of the table. The simulation model validates that the gyroscopic couple is a vector quantity. Figure 10 shows the built model in a MATLAB -Simulink Multibody Dynamic environment.

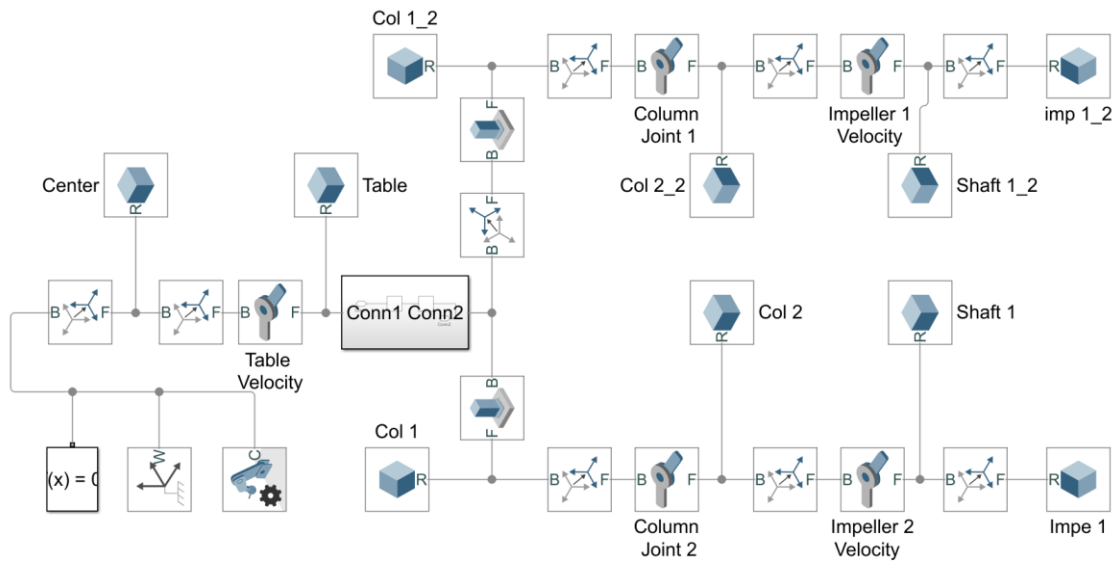


Figure 10 Multibody Dynamic Model for Identifying the Direction of the Gyroscopic Couple

The output of the above model can be seen in Figure 11. Gravitational force is applied in the downward direction. Proper spring and damping coefficients are applied to keep the impeller axis horizontal when the table is not spinning.

In this figure, clockwise motion of the table is appreciated when considered from the top. The rotating direction of both impellers is contrary to each other. Therefore, the direction of the developed gyroscopic couple is in the opposite direction but is expressed in the same in values. One impeller out of two is leaning from the inside, whereas the other is leaning from the outside. Both impellers are constructed in one model. Motion is applied to both impellers in the

opposite direction to understand that the gyroscopic couple is the vector quantity and depends on the direction of rotation of the impeller or table.

The output of the model has been represented in a simulated video, although for the purposes of illustration, one screenshot is represented in Figure 11.

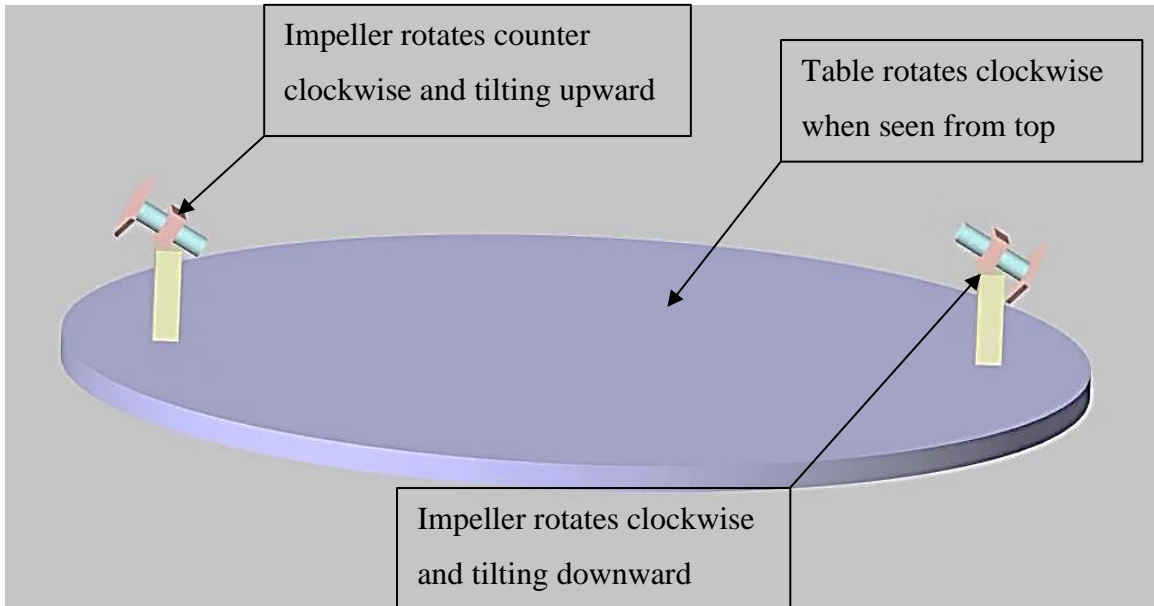


Figure 11 Visual Representation of the Simulated Model of Gyroscopic Couple Orientation in MATLAB

As shown in Figure 11, the gyroscopic couple reverses the direction in relation to any reversal of the rotation of the impeller or rotation of the table.

The second model simulates the real test environment. The model was created in the MATLAB-Simulink environment and input was given as per the actual test setup.

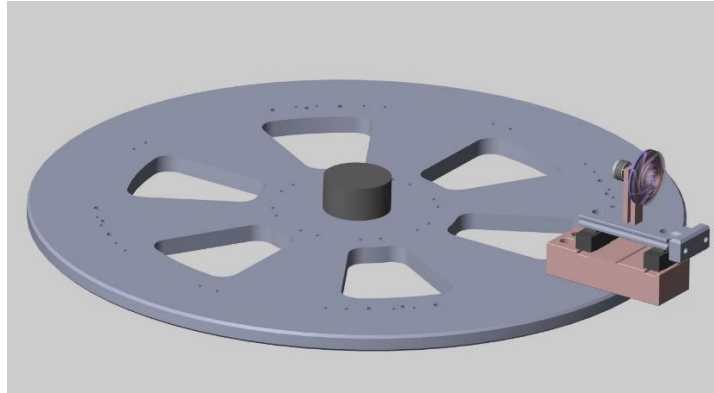


Figure 12 Test Setup Model Representation in the MATLAB-Simulink Environment

Figure 12 shows the physical representation of the model. Figure 13 represent the block construction in Simulink to get the output as Figure 12.

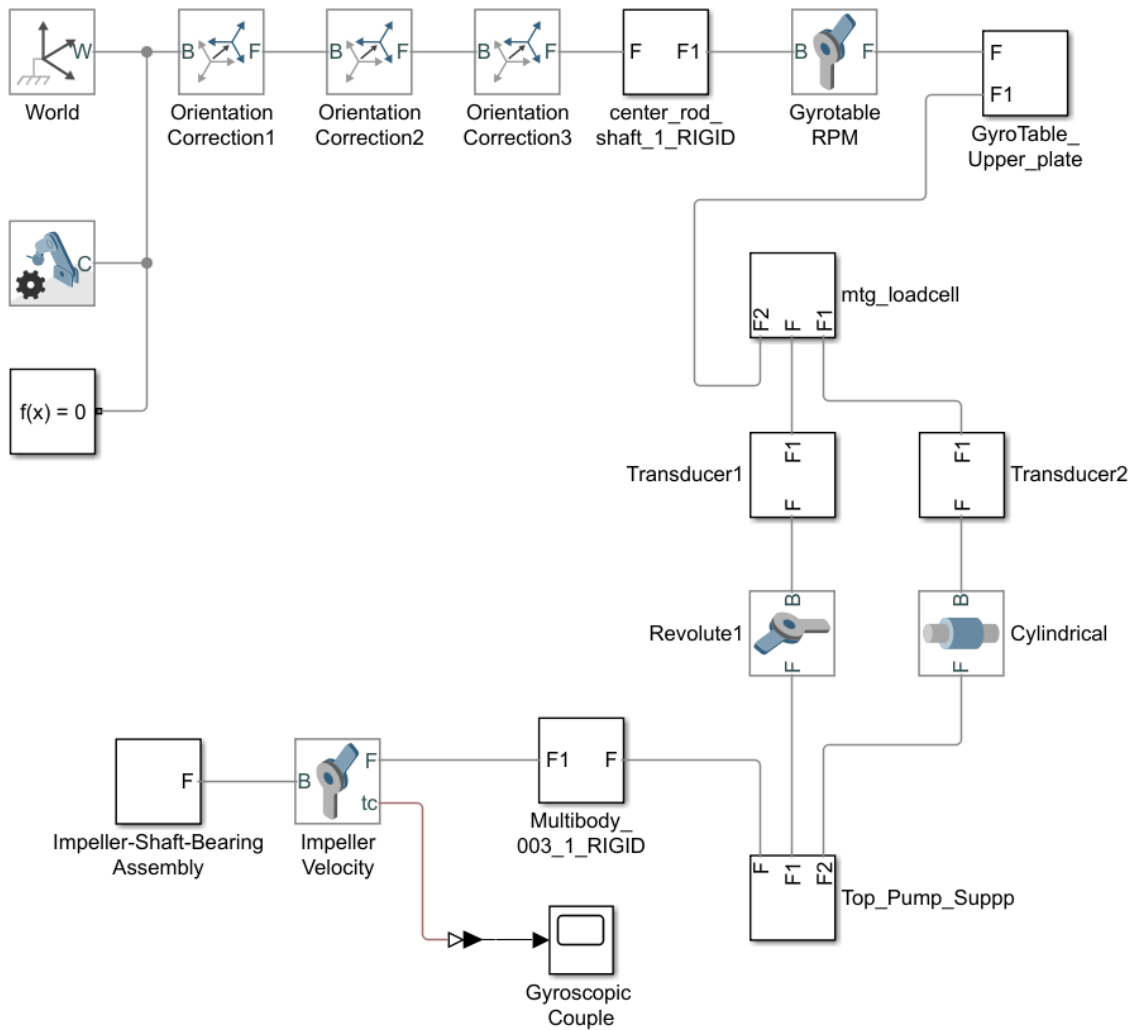


Figure 13 Backbone of the Model of the Test Environment in Simulink

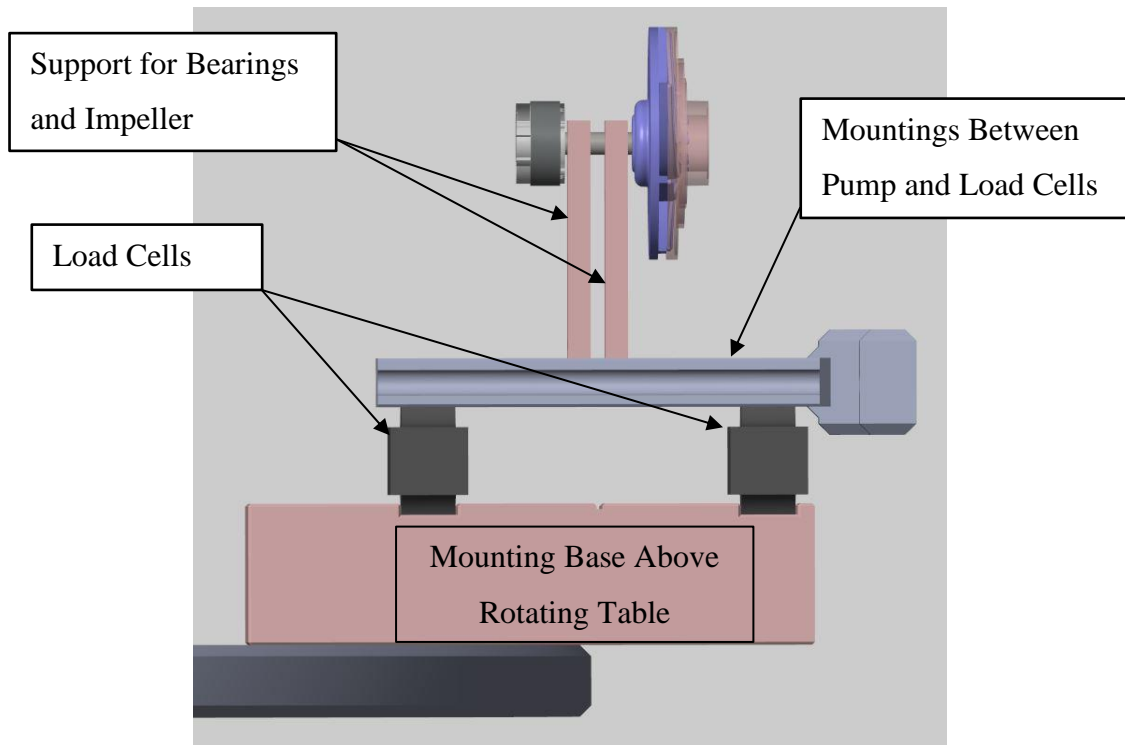


Figure 14 Detail View of Impeller Arrangement in the MATLAB Environment

Figure 14 represents the detailed view of the model arrangement in the MATLAB environment. The impeller and rotor of the motor are mounted on the shaft, and the shaft is passed through two bearings. Both bearings are supported by the loadcells (APPENDICES: B) with the help of “Support of bearing and impeller” and “Mounting between pump and loadcell”.

Both vertical mountings provide support to the shaft. These mountings help in the Simulink environment to measure the force acting during the test. These two vertical mountings are also replicating the casing of the pump in which bearings are supported. The whole setup is developed in Simulink in such a way that it can replicate the real-world testing situation. Therefore, from the simulated model, it is possible to receive more accurate values from the gyroscopic couple to the final application.

“Mounting Base Above Rotating Plate” provides support to the whole pump assembly and load cell assembly on the spinning table. Because of this support, the whole assembly can be mounted firmly onto the spinning table. Further information pertaining to the load cell is discussed in later sections.

Following this theoretical analysis of the system, the value of the gyroscopic couple is derived, and based on that value, the force acting on the bearing is calculated. The MATLAB-Simulink model also delivers similar values. Refer to Table 2.

Table 2 Gyroscopic Couple Values Comparison Derived by Simulation and Theory

Impeller Speed (RPM)	50,000	60,000	60,000	60,000
Table speed (RPM)	100	90	200	230
Gyroscopic couple based on theory (Nm)	0.087	0.095	0.211	0.242
Gyroscopic couple based on Simulink model (Nm)	0.083	0.09	0.2	0.23
Difference (%)	4.6	5.2	5.2	4.9

Table 2 shows the comparison between two gyroscopic couples. One is derived from the theory and other is simulated from the MATLAB-Simulink model. The values shown differ from each other by 5%.

3.3.3.2 Simulation for The Force Acting on The Bearing

Force acting on bearings is theoretically calculated in section 3.3.2.2. To validate the theoretically calculated force, one simulation was developed into commercial Finite Element Analysis (FEA) Ansys Software.

The CAD model was imported into the Ansys environment. Following this, the theoretically derived value of the gyroscopic couple was applied to the FEA model. The bearings were supported in the FEA model in a similar way as pump casing supports in an actual model. Therefore, the developed simulation in the FEA environment replicates the condition of the rotating components in the physical world.

Analysis was carried out after applying appropriate boundary conditions, which are discussed below, along with the results of the simulation.

Due to the limitations of the academic license, a simplified model was built by eliminating unnecessary parts from the CAD model. Figure 15 represents the simplified model for the FEA and illustrates two mounted bearings on the shaft. Moreover, grooves from the bearings and some fine curves were eliminated to make a simplified model that complied with the available academic-

license of Ansys. With fewer curves and grooves, the CAD model does not require the higher number of “nodes” and “elements” to generate mesh.

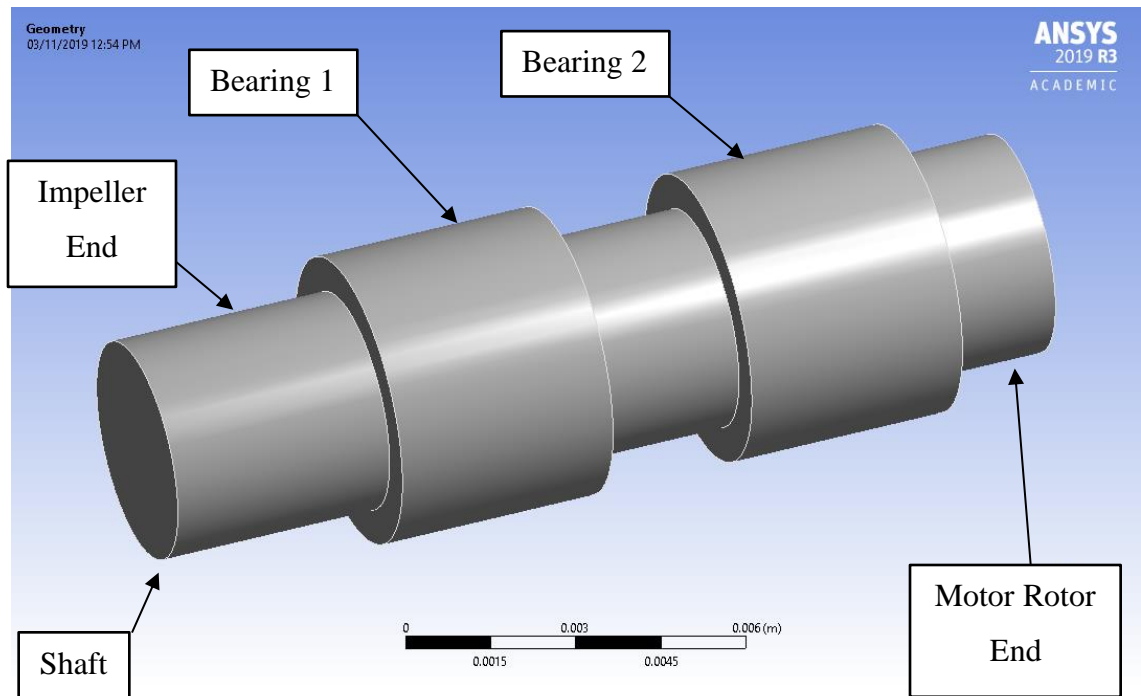


Figure 15 Simplified CAD Model for FEA

Refer Figure 16, for generated mesh into Ansys model.

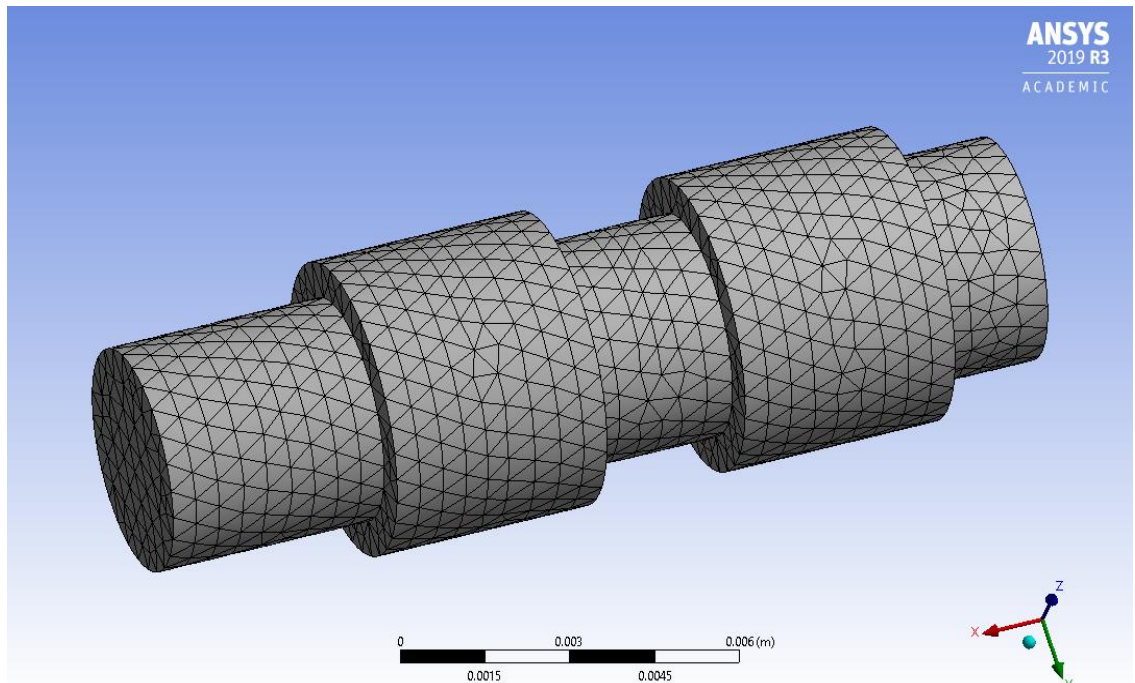


Figure 16 Meshing in Simplified Model For FEA

“Body Sizing” mesh was utilized to generate mesh for the simplified CAD model. The element size was 0.5 mm. Total Nodes and Elements were 29,027 and 19,593 respectively.

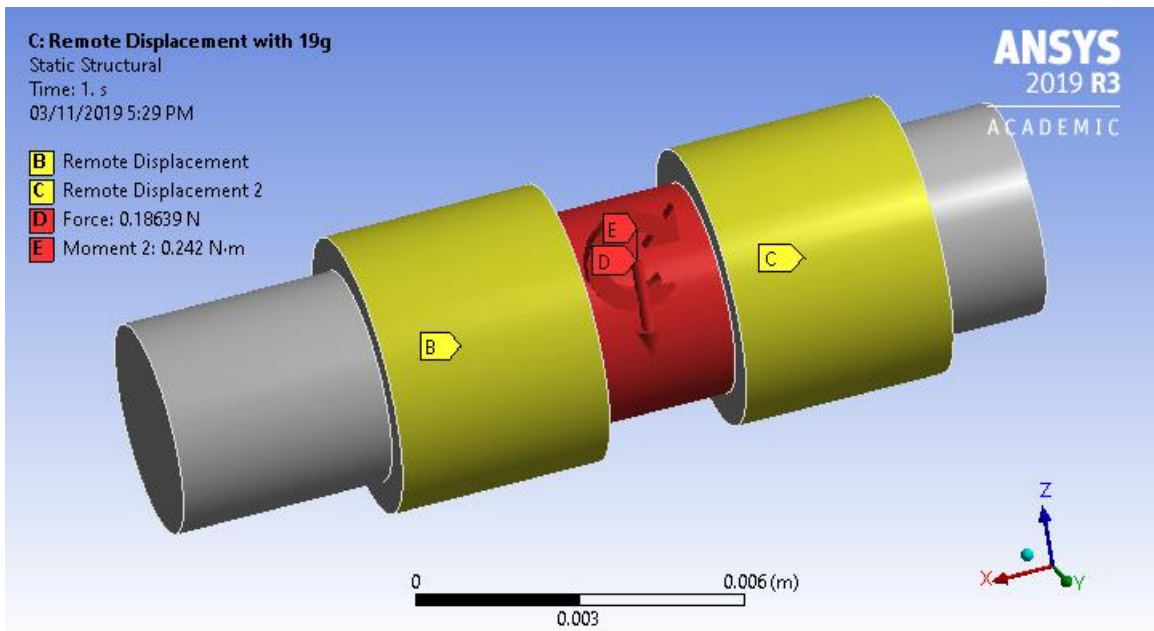


Figure 17 Boundary Condition Applied to the FEA model

Figure 17, shows the applied boundary conditions based on real-world conditions. Bearings 1 and 2 were fixed using remote displacement. The downward force was applied to the Center of Gravity (CG) of the shaft which replicates the gravitational force due to the mass of the spinning components. That was approximately 0.18639 N. The gyroscopic couple was also simulated by applying a moment of 0.242 Nm.

Three iterations were created to simulate the conditions. Those iterations were 90, 200, and 230 RPM of the spinning table by keeping the constant speed of the pump at 60,000 RPM. The results for the simulation tests are displayed in Table 3 and Table 4.

Table 3 Theoretical and Simulated Force Comparison on Bearing-1

Table speed	90 RPM	200 RPM	230 RPM
Force on bearing-1 by Theory (N)	14.26	31.80	36.59
Force on bearing-1 by Simulation (N)	14.25	31.87	36.57
Difference (%)	0.070	0.220	0.055

Table 4 Theoretical and Simulated Force Comparison on Bearing-2

Table speed	90 RPM	200 RPM	230 RPM
Force on bearing-2 by Theory (N)	14.45	31.99	36.77
Force on bearing-2 by Simulation (N)	14.42	32.06	36.76
Difference (%)	0.208	0.219	0.027

Table 3 shows the results of the force acting on bearing-1 and comparing the theoretical results and FEA-Simulation results. The difference between both results is shown in the percentage. Table 4 shows the comparison of bearing-2 theoretical and simulated data.

Therefore, since deviation in theoretical and practical values is less than 0.22 % the discussed theory is more firmly proven by comparing it with simulation results.

Chapter 4

Test Bench and Experimental Setup

4.1 The Purpose Behind Test Bench Development

Initially, a theory proposal has been discussed in this research, and theoretical results have been derived in order to determine the proposed theory. After that, various simulations have been carried out to provide more support for the theoretical calculations. After receiving successful results from the theory and simulation, it is necessary to do a practical test to validate the proposed method. This practical test can be carried out by developing a test bench that can generate the gyroscopic couple on the installed bearings in the pump.

Pumps can be tested on the test bench with set parameters. Below are the parameters for the test bench development that have been selected to validate the theory that the test bench can perform practical ALT test of the bearings:

- Validate the proposed method of ALT of the bearings;
- Measure the force acting on the bearings by the indirect method of the load cell;
- Test all 8 pumps simultaneously, as the test bench has the capability to mount 8 pumps at a time;
- Test the pumps on a test bench that has a table on which pumps can be mounted firmly and that can reach a rotational speed of 210 RPM, with the ability to control the rotating speed of the table in multiple steps; and
- Collect high-resolution electrical current from the BLDC motor and be able to store it in an adequate medium.

4.2 Construction of Developed Test Bench

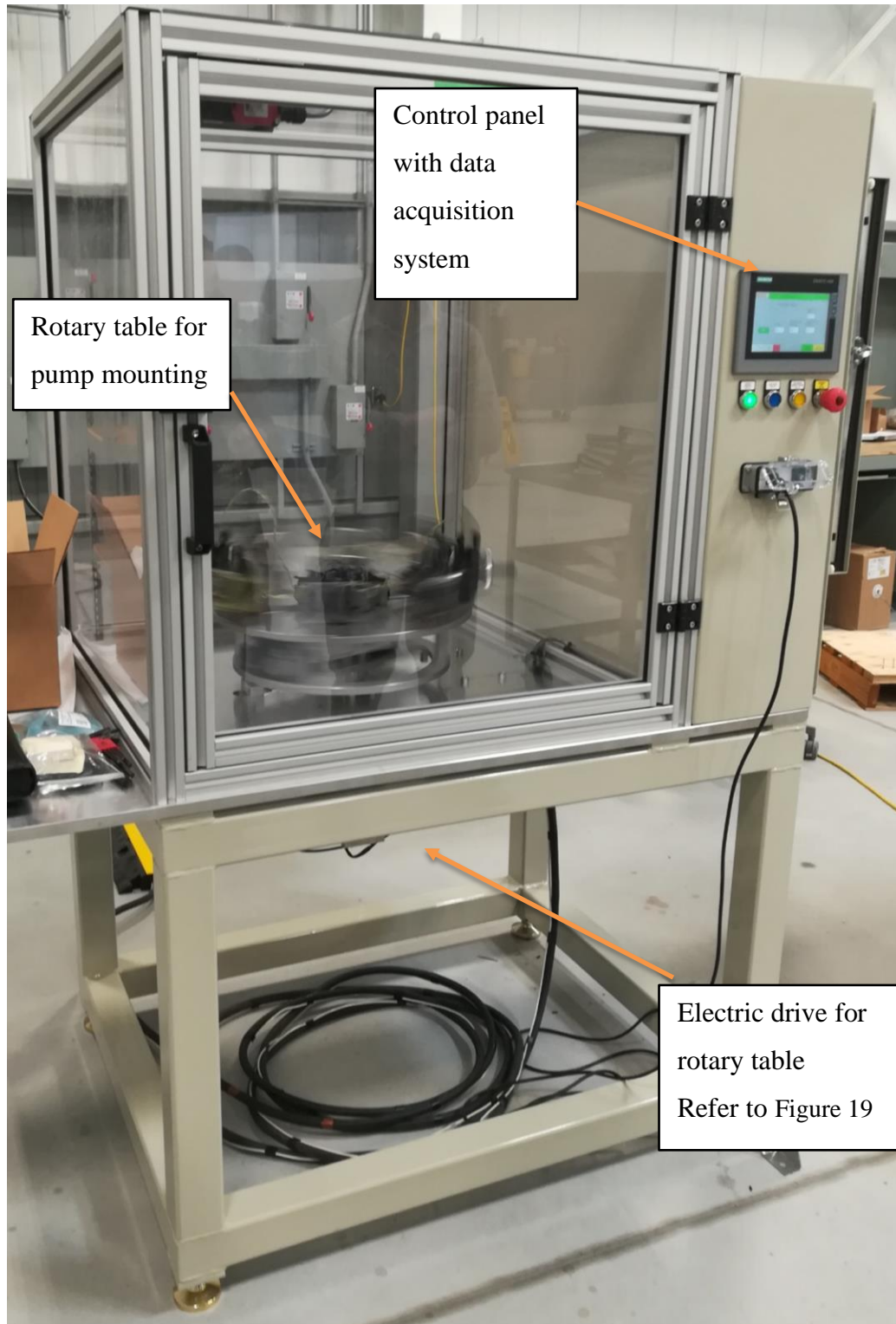


Figure 18 Developed Test Bench[6]



Figure 19 Electric Drive Unit for Rotary Table

As shown in Figure 18, the test bench has an enclosed chamber equipped with one rotary table. Due to product confidentiality, the complete detailed view of the rotary table is not displayed. However, the rotary table is similar to Figure 12. It can mount 8 pumps simultaneously and is also equipped with 8 fixtures to mount 8 pumps.

The test table has one control panel with the controller of an electric motor for speed control. In addition to the motor controller, the control panel is equipped with a data acquisition device from National InstrumentsTM. The controller can drive the motor up to 110 RPM. NI-9205 is used for data acquisition, which can collect 10 V (+/-) at a maximum rate of 250 kilo samples per second and can support 32 channels. Based on the test bench requirement, only 8 channels are used at a time.

Figure 19 represents the bottom part of the test bench. It is equipped with an electric motor drivetrain. The drivetrain transfers the motion to the rotary table by means of the belt drive system. The motor can reach a maximum of 110 RPM. The driver to driven pulley ratio is set to two. Therefore, the rotary table can reach up to 220 RPM. This spinning speed of the table is sufficient to generate the required gyroscopic couple.

The test bench can measure the electrical current from each pump. The table spins continuously, and the pumps are mounted on the table. This arrangement requires a special system that allows the electrical current to pass from the 200 RPM rotating table to the data acquisition (DAQ) system. The electrical current is measured by arranging the 0.01 Ω resistance in parallel. This type of arrangement of the resistance is also called a shunt and these shunts are arranged on the rotary table.

Each shunt must be connected by two cables with a DAQ unit. If four pumps are analyzed by the DAQ unit, then eight cables should be connected to the DAQ unit. However, it is not possible to connect eight cables directly to the DAQ unit as the table is rotating continuously. If cables are connected directly, then the table cannot rotate beyond several spins. However, in this case, the table is required to rotate continuously at 200 RPM for approximately 350 hours. Therefore, sliprings are introduced as an effective type of slip contact with rotating rings that allows the electrical current to pass through them. Figure 19 shows a stack of slip rings.

For this test bench, 14 sliprings are used to transfer the electrical signal or electric current. One slipring can withstand up to a maximum of 6 A of electrical current. Sliprings are able to connect multiple cables to the exterior of the rotary table. For further details of the sliprings, refer to Figure 20, where two cases are discussed. In option “A”, two parts are connected with the cables, and it is not possible to rotate the table in a single direction beyond a restricted number of revolutions, as the cable will break after a few rotations. In the case of “B”, components are connected with sliprings with no possibility with wire breakage. Therefore, in case “B”, the table can rotate in any one direction continuously for many numbers of rotations. There is one drawback to the slipring: the collected electrical current is noisy because of the sliding metal contact of the sliprings. The nature of the application may determine the degree to which this noise affects the final readings.

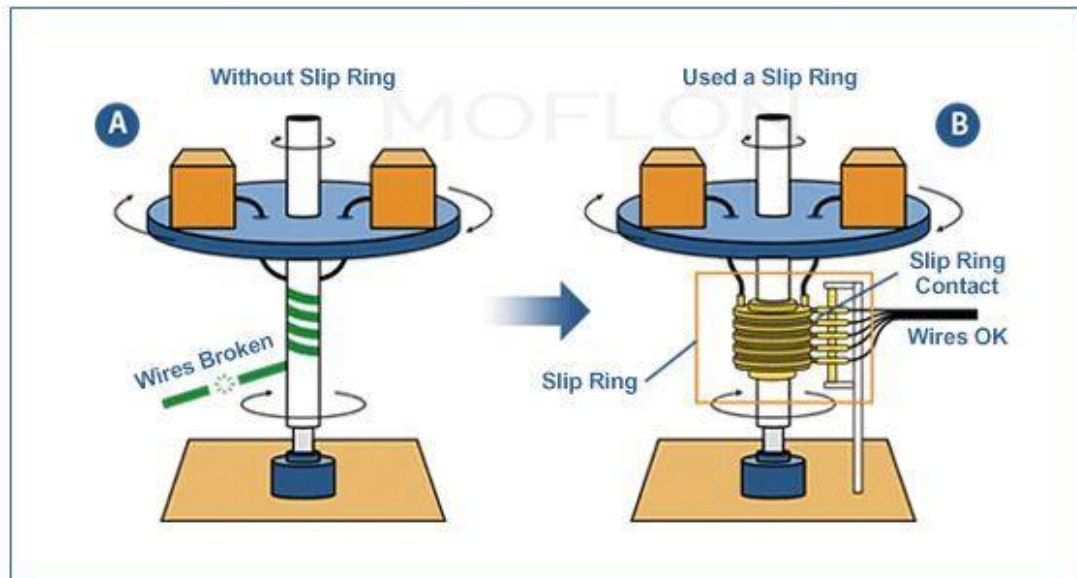


Figure 20 Slip Ring Schematic[22]

Electrical power supply is required to run the pumps on the spinning table. Each pump requires 12 V, 5 A DC power supply. The table can accommodate a maximum of 8 pumps at a time. The purpose of the slirings is to transfer the measured electrical signal from the pump to the outside of the rotary table and supply the power to each pump.

The testing table has two limitations related to slirings: the limited available number of slirings and the current carrying capacity of each slirping. For electrical current measurement, two slirings are required on each pump. If DC power is given to each pump from the slirings, then two slirings are not capable of drawing the adequate electrical current that can run more than 2 pumps. This restriction is due to the current carrying capacity of each slirping, which is limited to 8 A. Each pump requires DC 12V-6A continuous power. Therefore, instead of supplying the DC power to each pump from the outside of the table by utilizing more than 2 slirings, only 2 slirings are utilized to supply the AC power to the onboard Switched Mode Power Supply (SMPS) unit. SMPS converts the 110V-3A to DC 12V-25A. By using only two slirings, power can be supplied to 4 pumps instead of using 8 slirings. It keeps 6 slirings vacant to transfer the measured electrical current from the pumps. Generated DC power from the onboard SMPS is distributed to 4 pumps.

Refer to Figure 21 to understand the overall arrangement of all equipment for data collection and building the test bench.

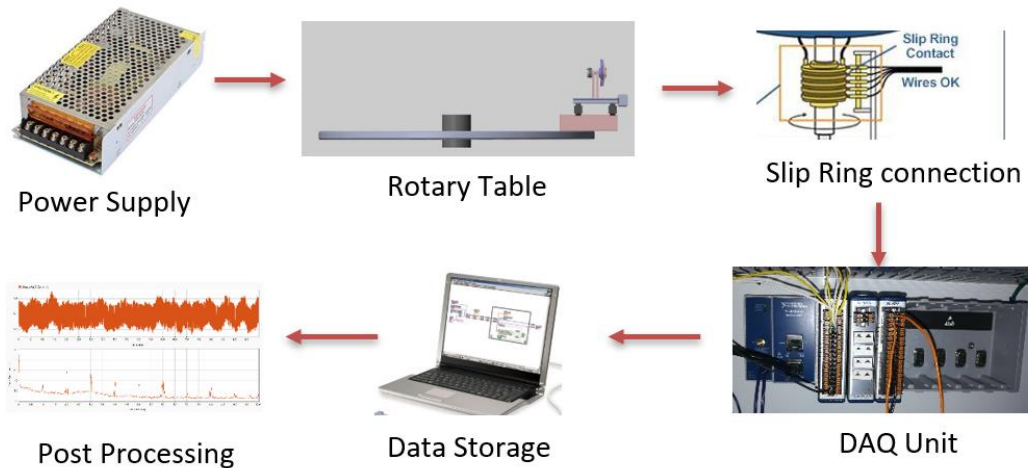


Figure 21 Testing Table Equipment Schematic Arrangement

Many types of equipment are used to build the test bench, but only functionally useful equipment is described. First, the SMPS unit converts the 110 V AC power to 12 V DC and distributes it to every pump. Every pump is connected through slirings to a DAQ unit. Then, this DAQ is connected to one laptop equipped with LabVIEW™ software. This computer is used to collect the

relevant electrical current data in a proper format. All data is also saved on the same computer hardware. Next, stored data were manually transferred or sorted for the post-processing of the measured electrical current for the fault detection of the bearings.

As the test bench is measuring the electrical current of the BLDC motor with the help of the DAQ unit, electrical signal passes through the sliprings. There is potential for noise in the electrical current due to metal to metal contact in the sliprings. This noise may affect the status of fault detection in future studies.

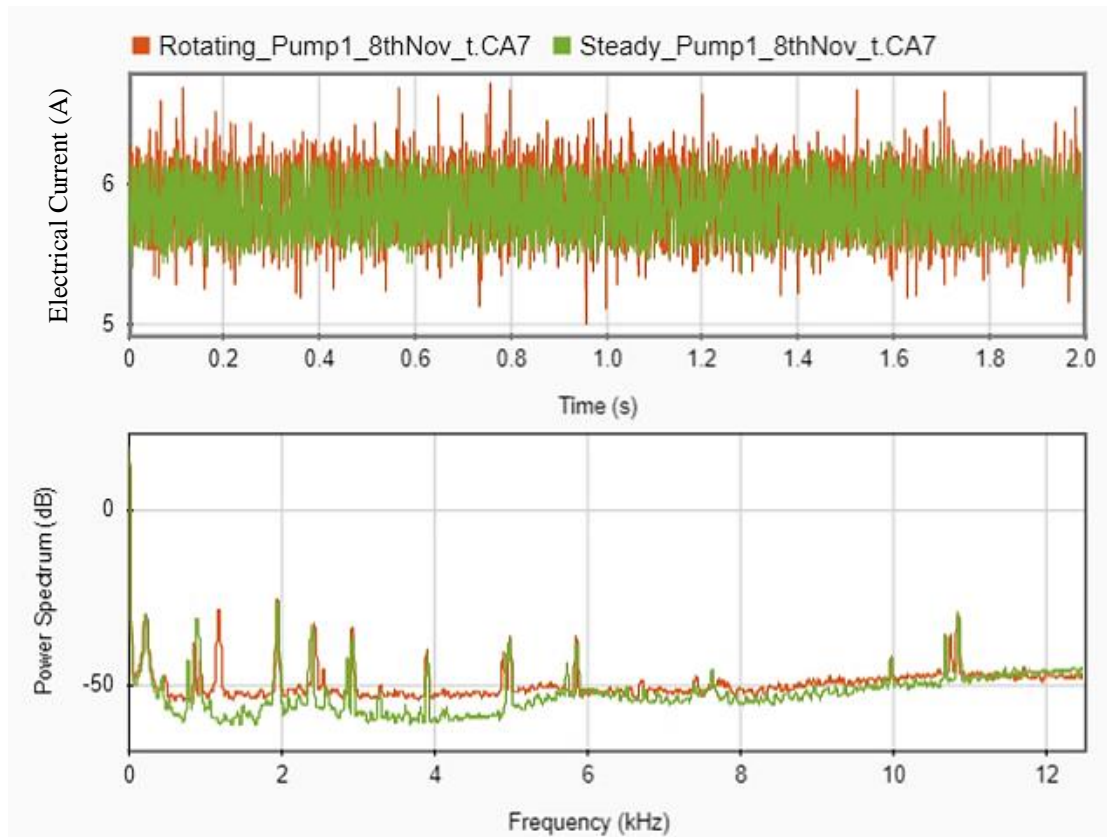


Figure 22 Presence of Noise Because of Sliprings

Figure 22 illustrates the measured electrical current from pump 1. The upper graph represents the electrical current measurement in the time domain, while the lower graph represents the frequency domain representation of the same electrical current. Power consumption of pump-1 is measured during the steady and spinning conditions of the table. The green line represents the electrical current measurement from the pump while the table was steady (a steady table means while the table is not rotating), and the orange line represents the reading from the same pump while the table was spinning. The readings are not identical, as some difference is present.

Small variations in measured electrical current are expected because of the presence of the gyroscopic couple while the table is in motion and because of the sliding contact of the sliprings. However, this minor difference in the measured electrical signal may affect the bearing fault detection. To be safe, electrical current is measured in both situations: with a steady table and with the table in motion. Both collected readings can be used for future studies on bearing fault detection.

4.2.1 Method for Measuring Electrical Current

For the bearing health monitoring, it is necessary to measure electrical current accurately with minimum noise. There are several ways to measure electrical direct current (DC). Here, two of them are discussed.

The first method is by connecting an ammeter in series with the circuit, as shown in Figure 23. In this method, the Ammeter is connected in series with power supply and load.

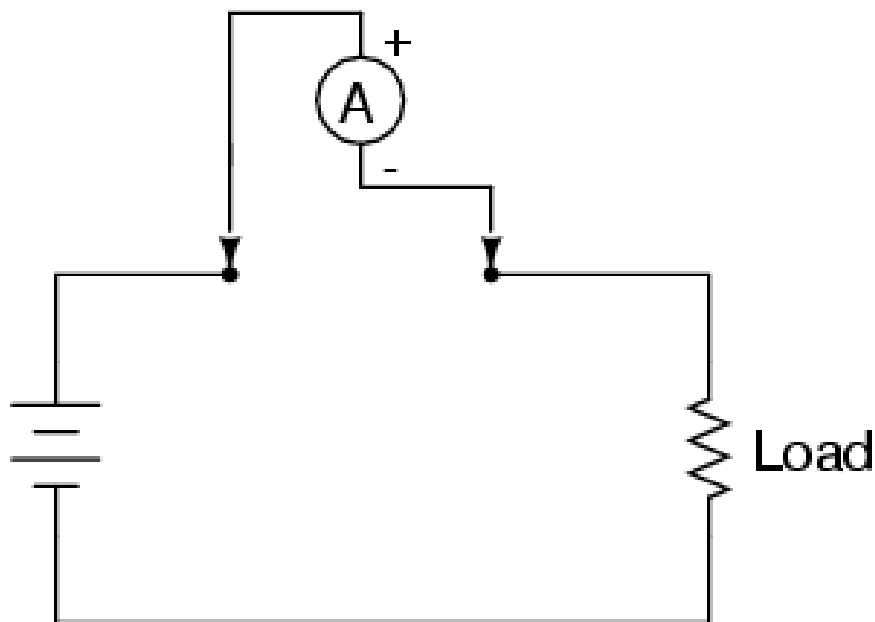


Figure 23 Electrical Current Measurement by Ammeter[23]

In Figure 24, the second method is illustrated; the voltmeter is used indirectly to measure the electrical current passing through the circuit or from the load. In this method, one small resistance is connected in series. Voltage across both ends of the resistance is measured. Based on the Ohm's law,

$$V = I R$$

Where, V = Potential difference across the resistance, measured in Volts

I = Electrical current passing through the resistance, measured in Amperes

R = Resistance value of the resistor, measured in Ohms

Given the value of connected resistance and voltage across the resistance, the value of electrical current passing through a resistance or load (in this case the motor of the pump) can be calculated.

In this test, 0.01Ω resistance is used.

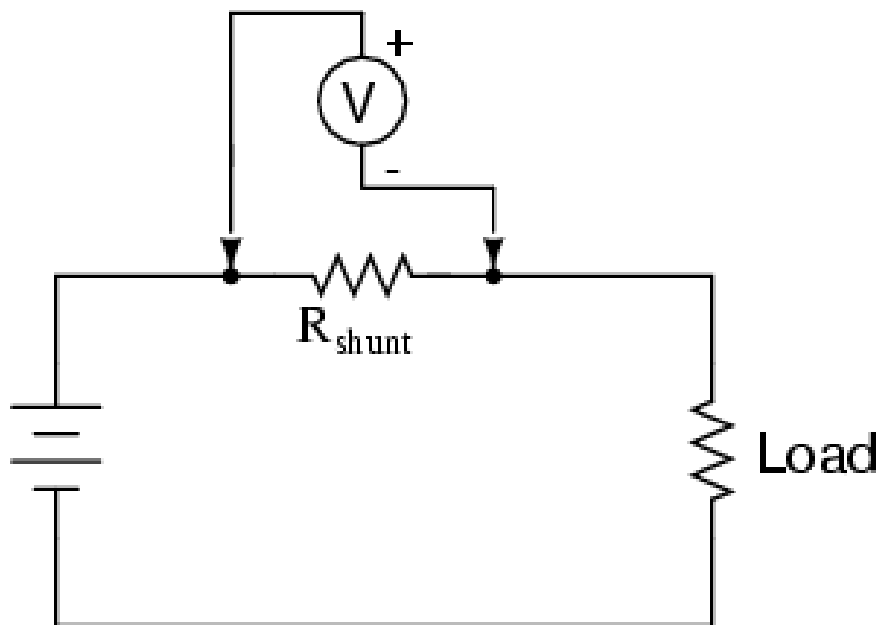
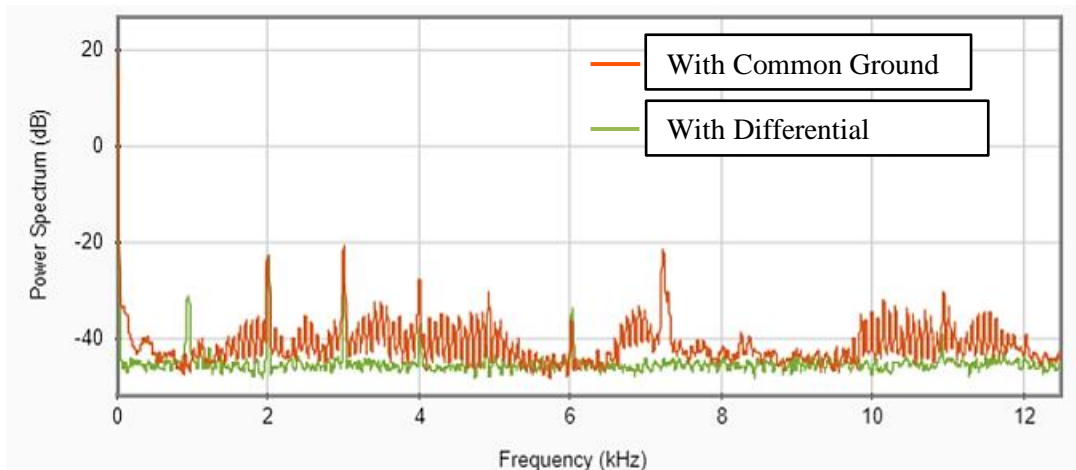


Figure 24 Electrical Current Measurement by Voltmeter[23]

Initially, one end of the voltmeter is connected to one end of the shunt, and the other end is connected to the common ground of the test table circuit. Measured electrical current from this arrangement is represented in the frequency domain in Graph 1 with a red line. The large amount of noise, which is above an acceptable level, can be seen from the graph.



Graph 1 Comparison of Electrical Current Measurement Methods

Following these measurements, an alternate connection of the components is carried out. In this arrangement, the voltmeter is connected across the resistance, which is called a differential arrangement. After this type of arrangement, the measured signal is plotted in the frequency domain, which represents a different signature with a drastic reduction in electrical noise. In Graph 1, the second set of data is represented by the green line and named “Differential Voltage”.

4.3 Various Tests on the Test Bench and their Results

The purpose of the test bench is to carry out various tests for validation of the newly developed methodology. Several tests are conducted on the test bench and discussed below.

4.3.1 Gyroscopic Couple and Load Measurement by Loadcells

Derived theory and simulation state that a gyroscopic couple occurs during rotation of the table and the gyroscopic couple transforms to the radial force on the bearings. However, the same should be proven by practical testing. Here, two load cells and two 3D printed fixtures are used to make specific arrangements to measure the force. This arrangement is illustrated in Figure 12 and Figure 25.

The pump is firmly fixed over the Mounting-1. Mounting-1 is fixed over the Mounting-2 by two load cells. The gyroscopic couple is generated between the two bearings and as a result, radial force acts on both of the bearings. This is discussed in further detail in section 3.3.2.2.

Since both bearings are assembled into the pump-casing, it is not directly possible to measure the force acting on the bearings. However, by providing the arrangement as shown in Figure 25, the

gyroscopic couple can be measured by load cells. The approximate value of the force can be calculated by resolving that couple over the span of the load cell. The distance between the bearings is 6.6 mm, whereas the distance between the load cells is 60 mm. Therefore, the couple is distributed across a greater span in the case of the load cell as compared to the bearings. Thus, the actual force measured by the load cell is less than the force acting on the bearings.

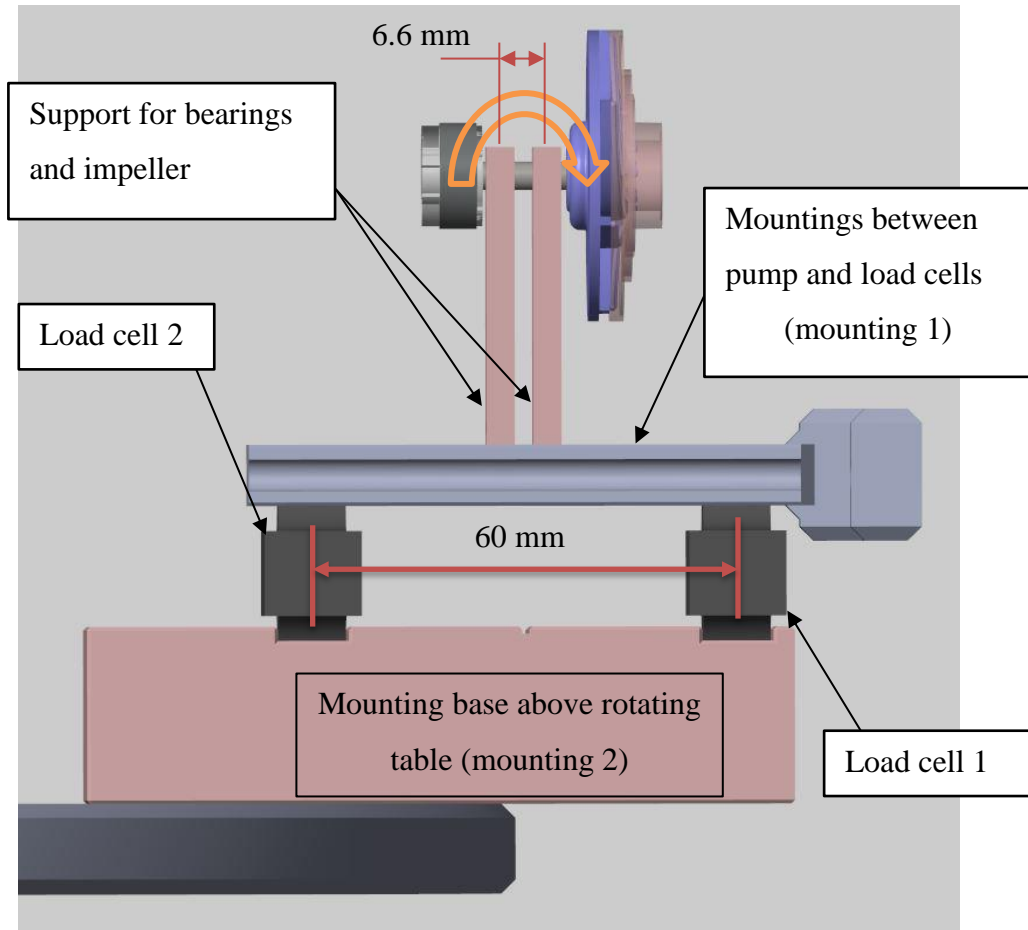


Figure 25 Detail View of Load Cell Test Configuration

To understand the actual loadcell (APPENDICES: B) configuration refer, to Figure 26. Because of the restriction over the product information, the image of the pump is cropped. Two long screws are visible in this image, and their function is to adjust the pump precisely over the Mounting-1 and to prevent sliding of the pump due to centrifugal force during table rotation.

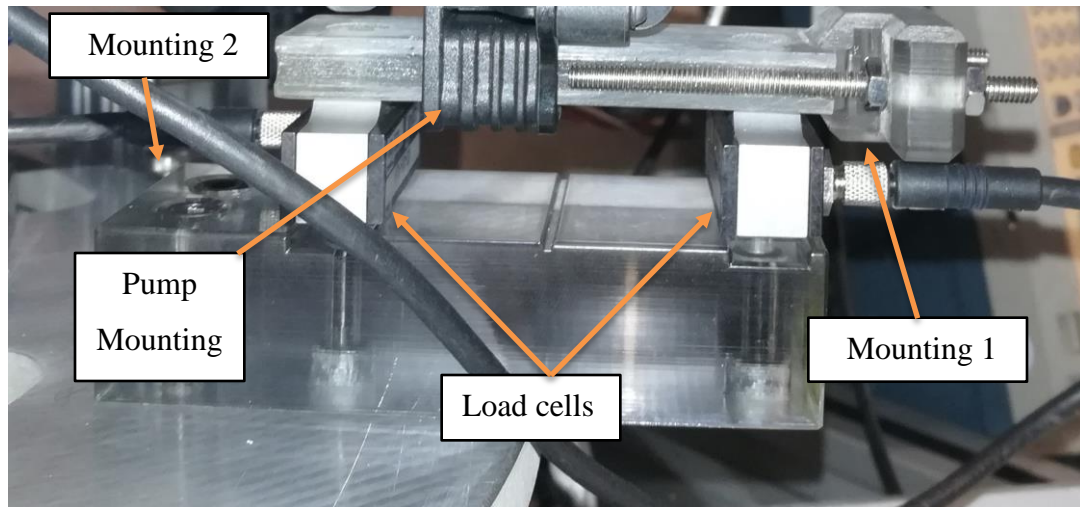


Figure 26 Actual Arrangement of Pump Over the Load Cells

4.3.1.1 Procedure of the Test

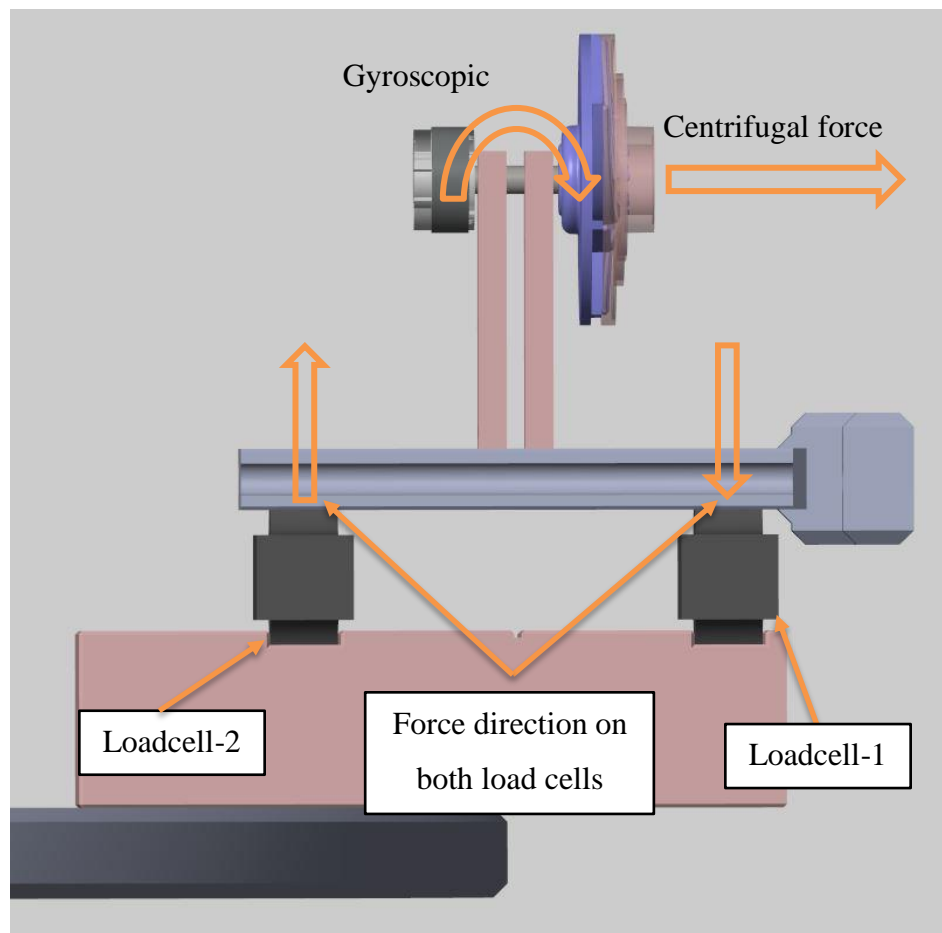


Figure 27 Force Acting During Testing

One specific procedure was followed to measure the force acting on the load cells. In this procedure, all components were mounted as per the above description and as shown in Figure 25. During the initial test, the table was started in the clockwise direction when seen from the top. In this initial stage, the pump was off: the impeller and relevant components were not spinning and only the table was spinning. Force was acting on the load cells; however, the value of the force was only due to the centrifugal force of the dead weight of the pump.

The second step of the test was followed after collecting results from the first step. During the second phase of the test, the table was kept in motion at the same speed and direction and the pump was started. Therefore, during the second phase, gyroscopic force was generated in addition to centrifugal force. Next, force was measured with the help of the load cells. In both cases, the measured values of the force were different because in the second phase, the gyroscopic couple was present in addition to the centrifugal force.

After the completion of the two phases of the test, there were two readings from each loadcell. The first reading was the result of centrifugal force, and the second reading from the load cell contained results from the centrifugal force and the gyroscopic couple. To extract the gyroscopic couple value from the reading, the first reading was subtracted from the second reading.

4.3.1.2 Testing result and outcome

During the testing, measurements were collected. During the first phase, the table was spinning at 100 RPM and the pump was off. The only centrifugal was acting on load cell-1. During the second phase, the table was kept spinning at 100 RPM and the pump was running on 50,000 RPM. Refer to Table 5, for further details on the force values.

Table 5 Readings from Load Cells

The Table Condition	Pump Condition	Load Cell-1 reading (N)	Load Cell-2 reading (N)
On	Off	7.43	-6.67
On	On	8.8	-8.45

Negative values in Table 5 represent the direction of the force on the loadcell. The force that acted on loadcell-1 was downward, and therefore the value is positive, while the force that acted on loadcell-2 was upward, and therefore the force is negative. The changes of the value of force on the loadcell-1 are due to the gyroscopic couple. The difference is 1.37 N (8.8 N–7.43 N). This value suggests the effect of a gyroscopic couple on the loadcell. Force is distributed over the 60 mm span

of the loadcells, although the span of the bearings is 6.6 mm. These measurements provide a distance ratio of 9.09. Therefore, the value of 9.09 should be multiplied with the force value to receive the force acting on the bearing.

$$\text{Force on bearing} = 1.37 \times 9.09 = 12.45 \text{ N}$$

The above value of force is derived from the practical test. However, force values on the bearings can be calculated from the discussed theory in the section 3.3.2.2. From the theory, the force value is 13.19 N, which is very close to the results from practical tests. The gyroscopic couple value can be calculated in a similar manner.

For calculating the gyroscopic couple, refer to Figure 27. Here, two forces were acting on two different load cells and generating the couple. Both forces are 60 mm apart. Values are somewhat different, but for simplicity, a value 1.37 N is taken to calculate the gyroscopic couple.

$$\text{Gyroscopic couple} = 1.37 * 0.06 = 0.0822 \text{ Nm}$$

Those values are compared and discussed in Table 6. All of the values are the result of conditions where table speed was 100 RPM and the speed of the pump was 50,000 RPM.

Table 6 Test and Theory Values Comparison

	Theory	Practical test	Difference in (%)
Gyroscopic Couple (Nm)	0.0877	0.0822	6.7 %
Force on Bearing (N)	13.2	12.45	5.9 %

From Table 6, results from the proposed theory (Table 1) match with values of the practical tests. The difference between the theoretical test and the practical test is less than 6.7%. This is an acceptable error in this research work based on the selected instruments for the measurements.

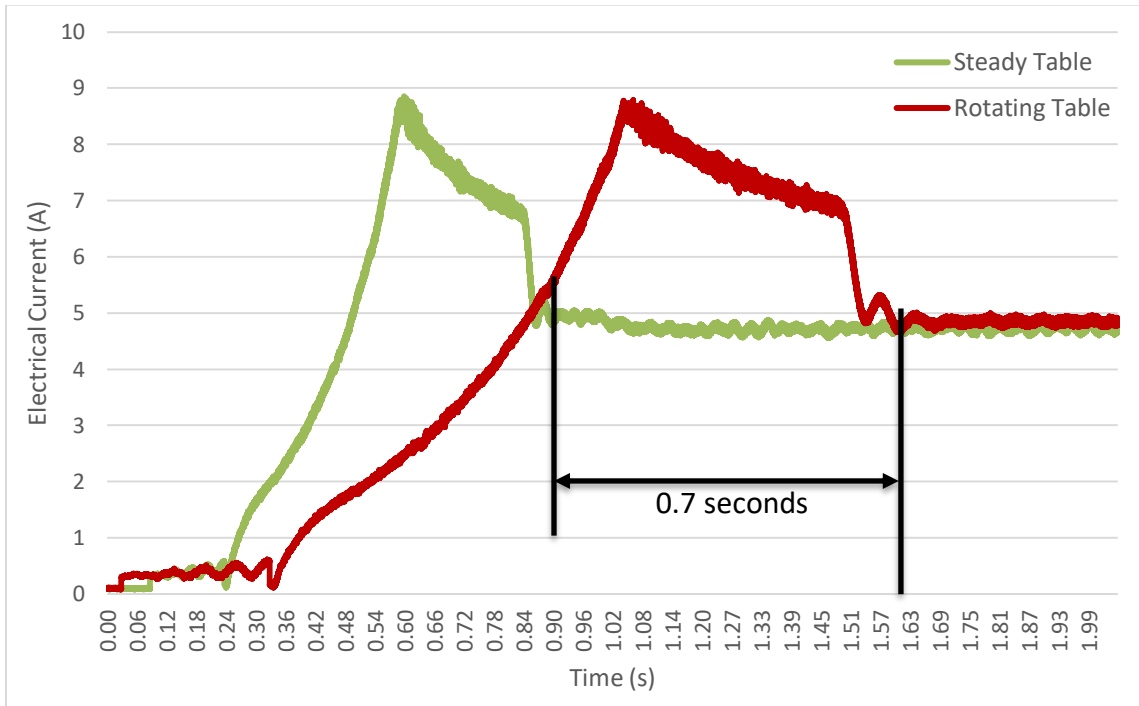
Therefore, this test proves practically that force acting on the bearing by the gyroscopic couple is the same as demonstrated in theory. This method produces a higher force on the bearings by generating a gyroscopic couple. The higher radial force expedites bearing wear, and that in turn leads to a decrease in the life of the bearings. Rapid wear helps to create an ALT of the bearings.

4.3.2 Trace of Higher Force on the Bearings from Electric Current Measurement

This section compares the electrical current consumption of the pump for two different cases. In the first case, the table was kept steady. During the second test, the table was kept spinning in the

clockwise direction when seen from the top. During both cases, the pump was kept running at the same speed.

During measurement of the electrical current, the DAQ unit was collecting 25,000 samples per second. Data were collected on 25 kHz frequency for the period of 2 seconds.



Graph 2 Electrical Consumption Comparison During Steady and Rotating Table

In Graph 2, the green line represents when the pump was running, and the table was steady. The red line represents the reading while the pump was running, and the table was spinning. The controller of the pump's motor is internally programmed such that it will not consume more than 9 A of electrical current during startup. Due to the rotation of the table, the more radial force applied to the bearings, the more the demand on torque from the motor to reach the same speed. The controller limits the demand of the electrical current; therefore, the motor takes more time to reach the pre-defined speed. This phenomenon is clearly visible from Graph 2. Here, the pump takes more time to reach a steady state of current while the table is rotating. The pump takes approximately 0.7 seconds more to reach the same speed as compared to the steady table. Moreover, the difference between average electrical current consumption by the pump in both cases is 0.27 A. This difference is because of the extra force on the bearings during table rotation.

This comparison proves that spinning components face extra force while the table spins. This additional force leads to the consumption of more electrical current from the motor, which is in line

with a previously discussed theory concerning the gyroscopic couple acting on the bearings while the table spins. This leads to an increase in the radial load on bearings and the bearings gradually wear out more quickly than the expected life.

4.3.3 Frequency Domain Representation of the Electrical Signal

For further monitoring of electrical consumption by the BLDC motor of the pump, measured time domain data is converted to frequency domain data with the help of MATLAB. The electrical current was measured in the time domain. It contains DC ampere readings over a period. In this test, 25,000 samples were collected for one second. Therefore, data is collected on a 25kHz frequency. This signal may have many combinations of frequencies. From frequency domain representation, it is possible to bifurcate the signal in the sub frequencies, which have been displayed in Figure 28.

As displayed in Figure 28, the top graph represents the electrical signal in the time domain. In that window, the X-axis shows time in milliseconds, and the y-axis represents the amplitude of the electrical current in amperes. The bottom graph represents the signal in the frequency domain. The X-axis in the bottom window represents the frequency distribution in 0-12 kHz. This graph shows that the collected electrical signal contains some higher energy frequencies at 1 kHz, 2 kHz, 3 kHz, 4 kHz, and 6 kHz. These higher energy frequencies can be understood by harmonics in the signal. They can also be described by first harmonics, second harmonics, and so on.

This signal was measured when the pump was running on 60,000 RPM, or 1000 revolutions per second. 1 kHz frequency can be directly related to the RPM of the motor. There are several tests that have been conducted by varying the speed of the pump, and each time, all of the harmonic frequencies also vary with the RPM of the pump.

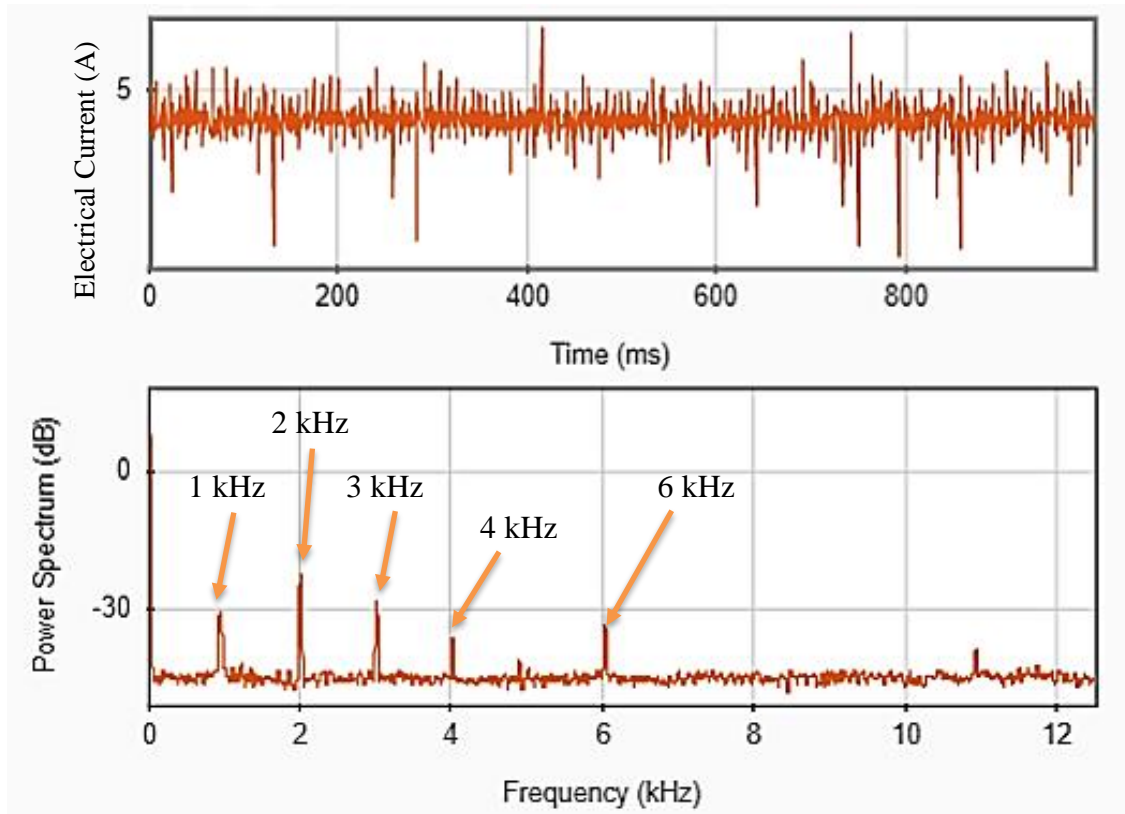


Figure 28 Frequency Domain Representation From MATLAB

The permanent magnetic rotor of the BLDC motor is equipped with two magnets. The rotor is spinning at 1000 revolutions per second. In other words, two magnets are spinning at a speed of 1000 revolutions per second. This spinning of the permanent magnet contributes toward generating the higher energy of 2 kHz. The motor is equipped with a three-pole stator. The rotor made with 2 magnets is spinning inside the three-pole stator, and it contributes the higher energy signal of 6 kHz.

The pump has an integrated controller with the BLDC motor. Electrical current is measured outside the controller. In other words, the controller is between the current measurement device and the poles of the stator. Therefore, the measured electrical current is not in the same pattern as passed through the poles of the stators. This difference may influence the fault detection of the bearings.

4.4 Tested Pump on Test Bench

One theory is discussed regarding the generation of the gyroscopic couple. This couple generates the higher force on the bearing that eventually accelerates the bearing wear. This theory is supported by relevant tests and simulated data. The theory of the accelerated life test of the bearing is discussed in the previous sections. Simulated data is also provided to support the theory. One

practical test was conducted to support the theory and prove the ALT of the bearing. Information pertaining to this test is presented below.

For the final test, two pumps were chosen. The speed of the table was set to 200 RPM, and pumps were set to 60,000 RPM. Two second long electrical current was measured at 30 minute intervals at the rate of 25kHz. One more reading was collected on every day while the table was not rotating. These collected readings were 2 seconds long at 25 kHz.

This test was designed to cause the bearings to fail at approximately 350 hours. The bearing manufacturer provided the value of force. This force can compress bearing life to 350 hours. According to the theory, this suggested amount of force can be generated by a gyroscopic couple while the table is rotating at 200 RPM. Therefore, the test was designed by considering theoretical values and data provided from the bearing manufacturer to cause bearing failure at approximately 350 hours.

For testing purposes, two pumps were chosen. During the test, bearings from both pumps were caused to fail. Bearings from one pump showed failure in 290 hours and those from the second pump showed failure in 330 hours. Therefore, the research aim is fulfilled: the normal life of the bearings is 8000 hours, but ALT reduced it to approximately 300 hours.

Chapter 5

Summary, Conclusion and Future Work

5.1 Summary

This research focuses on accelerated lifetime testing (ALT) of the deep groove radial ball bearings for one application based on the specific product target. The objective of this research is mentioned in section 1.3.

In this research, one new approach is proposed for an ALT of the bearings with the help of a gyroscopic couple. In this method, one test bench is developed that generates conditions such that high-speed spinning bearings experience a higher radial force because of the gyroscopic couple. This generated gyroscopic couple contributes to rapid wear of the bearings before their expected lifespan in ideal working conditions.

In the initial part of this thesis, theoretical evidence (section 3.3.2) is presented for the proposed method. Then, simulation (section 3.3.3) is carried out to support the theory. In addition, a test bench is built to carry out the final test of ALT of the bearings. This test bench is utilized to carry out a sequence of testing (mentioned in section 4.3) that supports the results from theory and simulation.

5.2 Conclusion

From the proposed theory and simulation, it can be determined that the ALT of the bearings is possible by considering the required constraints and conditions. A list of constraints and testing requirements is mentioned to carry out ALT of the bearings. By considering these factors, a unique testing method is proposed in this thesis. Theories and simulations are described to prove the viability of this proposed new method.

In the described theory, the higher radial force on the bearing is applied by generating a gyroscopic couple. The high-speed spinning components are effective in generating an adequate gyroscopic couple. The value of this couple and radial force on bearings is derived from the theory and then compared with simulation results obtained from the MATLAB-Simulink multi-body dynamic model. For further verification, the indirect force acting on the bearings is measured with the help of a loadcell. Thus, the value of force acting on the bearings is derived and validated by three methods: theory, simulation and practical tests. In summary, the outcome from all three methods is similar and the results of the methods validate each other.

To summarize all of the values in a single table, a test was carried out by keeping the speed of the table at 100 RPM and the pump speed at 50,000 RPM. Table 7 shows the outcome from all three methods. The table demonstrates that the derived values of force from all three methods are proximate to each other and validate the overall method and test.

Table 7 Force Comparison on the Bearings by Various Methods

Force on bearing-1 by Theory (N)	13.2
Force on bearing-1 by Simulation (N)	13.9
Force on bearing-1 by Practical Test(N)	12.45
Force on bearing-2 by Theory (N)	13.3
Force on bearing-2 by Simulation (N)	14.12
Force on bearing-2 by Practical Test(N)	14.47

Therefore, this proposed new method is not only proved by theory but supported by simulation and practical results.

A test bench was developed for testing installed bearings in the pump. As discussed, it has the capacity to mount 8 pumps simultaneously. Initially, two pumps were tested. Bearings from both pumps failed within 290-350 hours of running (Section 4.4). The expected life of the bearing is 8000 hours. Bearing testing time under previous methods was 2500 hours. Using this acceleration testing method, it is possible to compress the bearing testing time from 2500 hours to approximately 350 hours.

In addition to this test, three methods of the fault detection of bearings are discussed. Out of these three methods, the EMD topic is explained in section 5.3.1.3. The method discussed with the EMD tool can clearly indicate the faulty bearings on the scatterplot. Here, electrical current consumed by the BLDC motor is analyzed to detect the fault of the bearings. However, fault detection is not a primary scope of this research. Therefore, all three methods are discussed very briefly. Further work should be carried out in order to pursue future research on fault detection of the bearings.

Finally, it can be concluded that this research proposes and successfully validates a new method for the ALT of the bearings.

5.3 Future Work

The long-term goal of this research is to identify and monitor the health of bearings with the help of the electrical current consumption patterns of the BLDC motor during ALT.

Here, a test bench for ALT of the bearing is developed and validated with support of the theory. During the development of the test bench, one more feature was accommodated for future work. This is a provision for collecting a high-resolution electrical current from the BLDC motor of the pump. At a preliminary level, three methods are discussed for the fault detection of the bearings.

5.3.1 Fault Detection of the Bearings

Fault detection was not the focus of this thesis. However, for providing support to future studies, some preliminary work was conducted toward fault detection of the bearings. The major target for future research is to detect the fault of the bearing by analyzing the electrical current measured from the BLDC motor that drives the pump.

Three methods are used to identify the bearing health. The first is based on the vibration measurement and the other two are based on the measured electrical current from the motor.

5.3.1.1 Bearing Degradation Detection from Vibration Signal

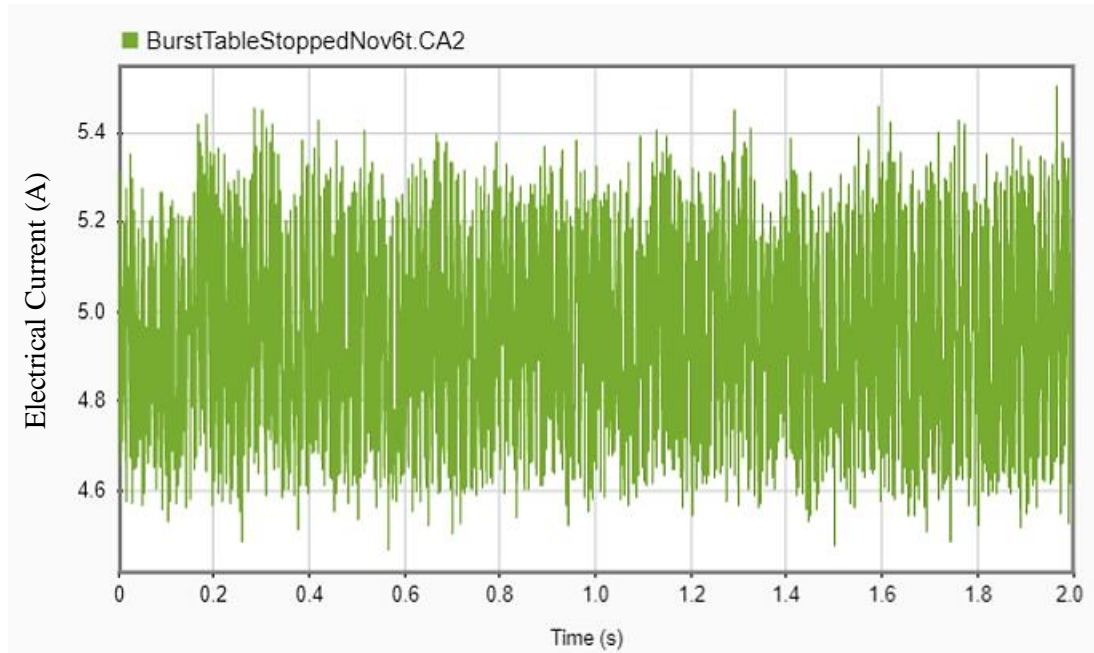
Sample of studies on vibration-based fault detection of the rotating components are discussed in section 2.1. The faults of the bearings can be detected efficiently from their vibration signature[14]. There are many advantages to the vibration-based fault detection methods, which enable the detection of the location of a fault in the bearings. To verify the degradation of the bearings, vibration signatures were collected before and after the failure of the bearings.

The pump was rotating at the speed of the 60,000 RPM, or 1000 revolution per second, and therefore, 1kHz was selected as a reference for the measurement. Before starting the test, the vibration signature was measured, and it was 3.15 m/s^2 at 1 kHz. When the vibration signature was measured after the failure of the bearing, it was increased to 17.27 m/s^2 .

The faults of the bearings can be detected based on the steeper value of the acceleration by analyzing the vibration signature of the bearings. Analysis of the vibration signature is not under the scope of the thesis; therefore, only a brief overview of the vibration analysis is represented instead of a detailed analysis.

5.3.1.2 Bearing Fault in Frequency Domain Representation

The frequency domain depiction is a representation of the measured time domain signal on the graph of energy-frequency. The X-axis of the graph represents the range of the frequency and the Y-axis represents the energy level of the frequency on the decibel scale.

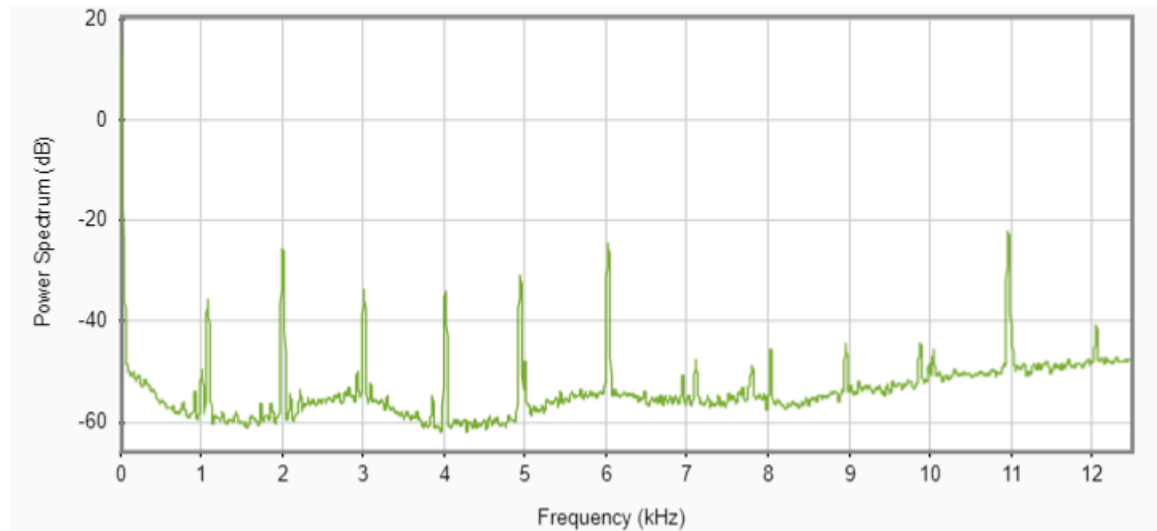


Graph 3 Representation of Measured Electrical Signal in Time Domain

Based on the previous discussion, the BLDC motor of the pump is equipped with a three-pole stator. One controller is integrated with the motor. The function of the controller is to generate the proper frequency for all three poles of the motor in order to control it. During the test, the electrical current was measured outside of the motor. Therefore, the same frequency or electrical current cannot be measured. Ideally, traces of the frequency should not leak outside of the controller. However, the DAQ unit measures the blurry signature of the generated frequency by the controller. Prior to conducting this test, it was hypothesized that a defective bearing may provide some indication of its deficiency outside of the controller. Hence, fault detection of the bearing by electrical current analysis is proposed.

The measured electrical current outside of the controller contains many frequencies. It is not possible to identify the included frequency by representing the measured electrical current in the time domain representation. The measured electrical current from the pump-2 (pump-2 is the second pump of two tested pumps) in the time domain region is shown in Graph 3. From this graph, only the range of the amplitude of the electrical current can be identified. The electrical current

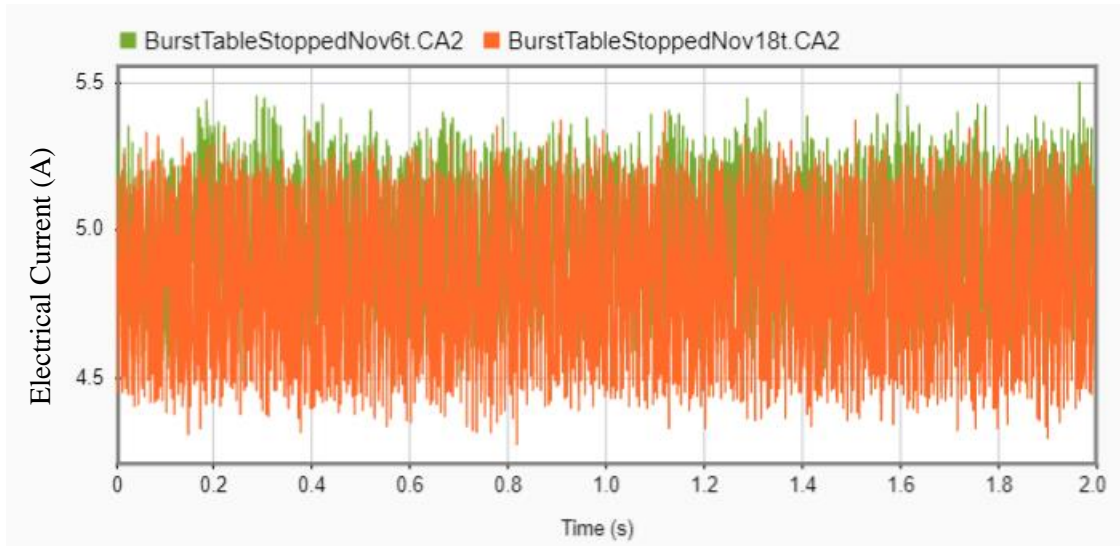
amplitude is between 4.6 A and 5.4 A. This graph is in time domain, which renders it difficult to extract additional information from it. The same reading is represented with frequency domain representation in Graph 4.



Graph 4 Representation of Measured Electrical Signal in Frequency Domain

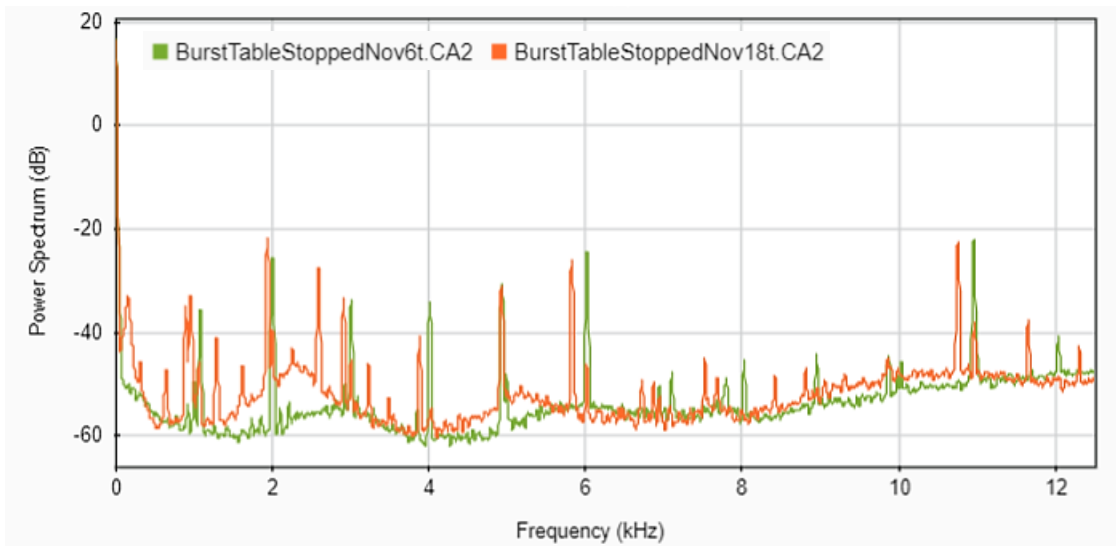
Graph 4 includes more information, it shows the included frequencies in the measured electrical signal and represents the energy level of those frequencies in decibels (dB). Therefore, representing the measured signal in the frequency domain graph releases more information pertaining to the signal.

Here, one example is taken to understand the importance of the frequency domain representation of the measured signal. Graph 5 is the time domain representation of the two electrical measurements from Pump-2. The first electrical signal was measured on 6 November, while bearings were in good conditions. It is represented with the “Green” line. The second reading was taken on 18 November. After running for approximately 290 hours, bearings are worn out near to the defective bearing conditions. The faulty signal is represented with “Orange” lines.



Graph 5 Fault Detection from Time Domain Electrical Signal

In the Graph 5, it is very hard to identify the difference between faulty and healthy bearings.



Graph 6 Fault Detection from Frequency Domain Electrical Signal

In Graph 6, however, the same measured electrical signals from Pump-2 are presented in the frequency domain. The green line represents the measured electrical current of Pump-2 with healthy bearings. The orange line represents the measured electrical current of Pump-2 with faulty bearings. These two signals are the same as Graph 5, but the difference is in the data presentation. Graph 5 shows the time domain representation, whereas Graph 6 shows the frequency domain presentation.

In Graph 6, the “Orange” signal with faulty bearings looks different as compared to the “Green” signal from the healthy bearings. Previously it was not visible in Graph 5, but because of presence of the fault some new harmonics exist as compared to the healthy bearings and it is visible in Graph 6. Mostly, each harmonic has a higher energy content as compared to the healthy bearings.

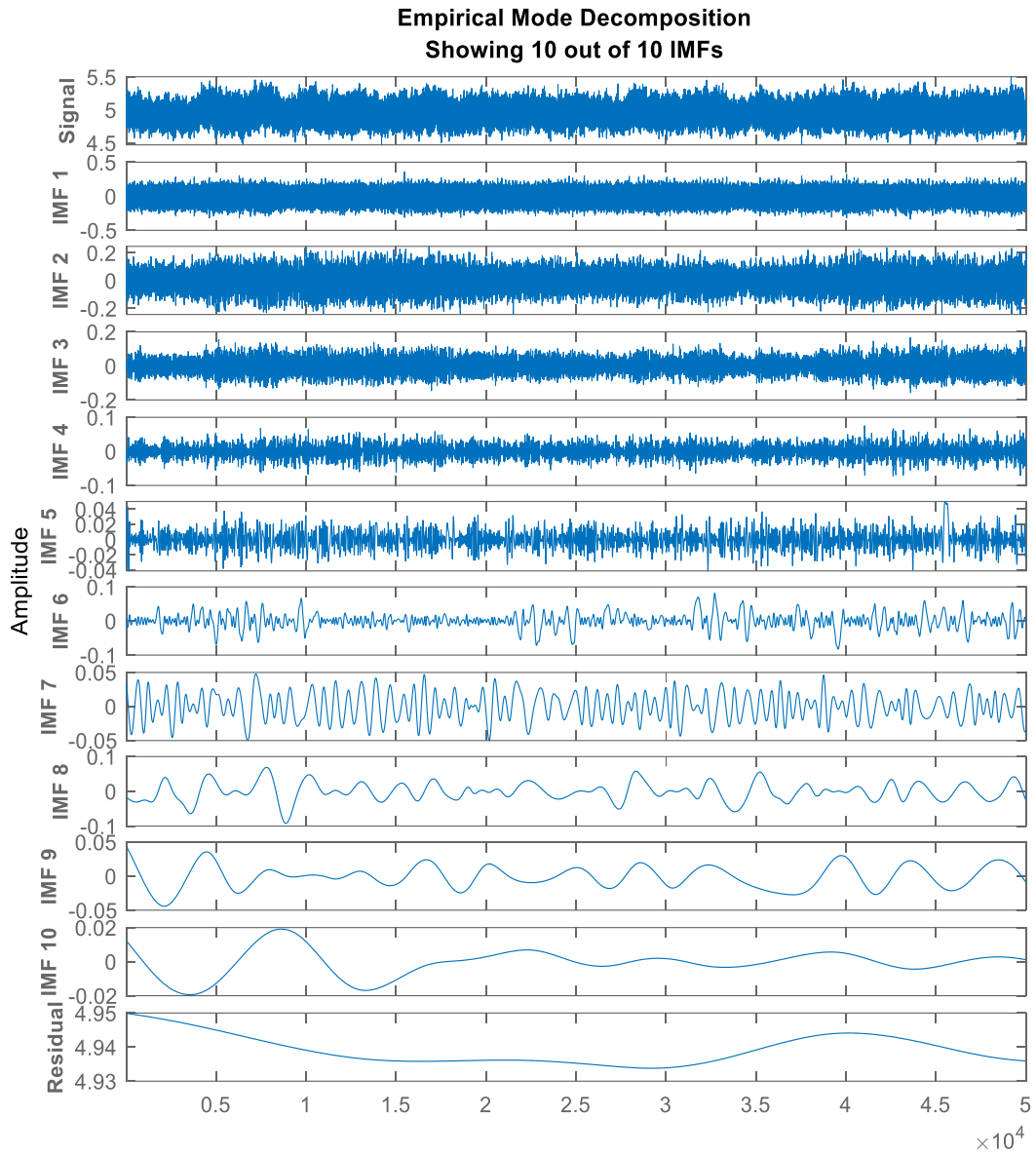
Graph 6 shows the measured signal in the frequency domain. Although it is not absolutely clear, but electrical current with faulty bearing is more visible with frequency domain representation as compared to the time domain representation.

5.3.1.3 Bearing Fault Detection with EMD

Empirical Mode Decomposition (EMD) adaptively and locally decomposes any non-stationary time series in a sum of Intrinsic Mode Functions (IMF). These represent zero-mean amplitude and frequency modulated components[25]. In other words, EMD separates the mixture of the original signals. EMD has numerous advantages with few limitations. However, one trial has been carried out to check the advantages from the EMD in this thesis.

With the help of MATLAB, 10 IMF are extracted from the measured electrical current of the BLDC motor. Referring to Graph 7, 10 IMF are generated from the electrical current of Pump-2. As electrical current is measured over the 25 kHz, each IMF contains 50,000 samples in the X-axis. Therefore, it is very hard to identify any high frequency signal from the IMF-1 or IMF-2. If any IMF contains the lower frequency, then it is visible from the rest of the IMF (IMF-7 to IMF-10). But if the pump is running on the 60,000 RPM, then the change due to bearing fault should be in IMF with higher frequency signals, and that is hard to determine from Graph 7. Although the traces of the faulty bearings are not visible from the graph of the IMF, but it may be included in the value of the IMF.

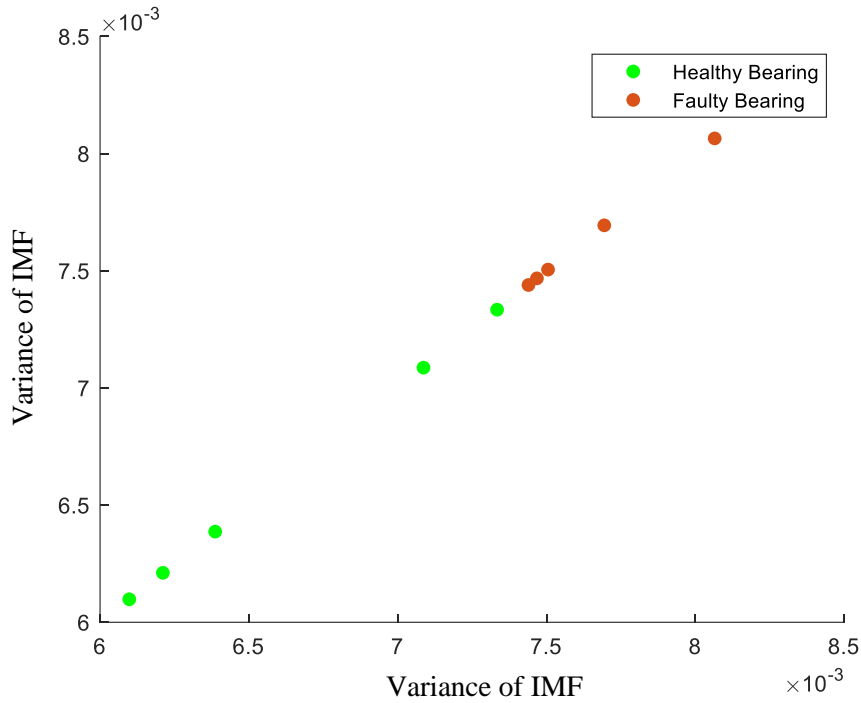
To identify the fault of the bearings from the electrical signal with the help of EMD, one function has been developed in the MATLAB: the output of the function is a scatter graph. It represents the healthy and faulty bearings in different groups. Script of the developed function is mentioned in the “[MATLAB Code](#)” under the Appendices.



Graph 7 Generated IMF from the EMD of Pump-2

The electrical current from each pump is measured by LabVIEW software, and data were stored in “.CSV” file format. MATLAB function reads all “.CSV” files. It makes a directory from files, arranging them in ascending order of the time and date. When the test was started, all bearings were healthy and at the end of the test all bearings were degraded. Here, the function selected some files from the initial time of the test and some files from the last part of the test. These collected files are kept separate for further calculations. When the scatter plot gave the output, the MATLAB function handles healthy bearings with “green” color and faulty bearings with “orange” color. With the help of the “for-loop”, data from each file is extracted. EMD is calculated, and all values of IMF are

stored in temporary files. Based on the input, any one IMF is selected out of 10 for the next process. Variance is calculated from the selected IMF from each file, after which calculated variance is stored in sequence. This stored variance is plotted with the help of the scatter plot and output is represented in Graph 8.



Graph 8 Scatter Plot of Healthy and Faulty Bearings

The MATLAB function distinguished faulty and healthy bearings on the scatterplot. Here, only the variance of the IMF is derived from each file. Therefore, both axes of the plots represent the same parameter. One-dimensional plots are possible; however, instead of the one-dimensional plot, a two-dimensional scatter plot is created for better representation.

Fault detection of the bearings is not discussed in detail here, as it is out of the primary scope of this thesis, although Graph 8 can briefly distinguish faulty and healthy bearings. By presenting three different methods for fault detection, a foundation is created for the future study of fault detection of the bearings.

In addition to the above work there are many algorithms available that can be applied to verify which would be most suitable for this application. Because of the presence of the controller between the stator of the BLDC motor and electrical current measurement device, it would be a difficult task to detect fault from the collected electrical traces.

There are few signal processing methods that can help to identify some abnormalities in the collected electrical signals from the BLDC motor. These may identify the difference between healthy and faulty bearings.

➤ Signal Processing Methods:

1. Fast Fourier Transform
2. Wavelet Transform
3. Wigner-Ville Distributions
4. Empirical Wavelet Decomposition
5. Empirical Mode Decomposition (as discussed in the section 5.3.1.3)

There are some new methods based on Machine Learning techniques.

➤ Machine Learning Methods:

1. Support Vector Machine
2. Novelty Detection
3. Artificial Neural Network

This research is concentrated on a specific application (product), but the principle of the use of a gyroscopic couple to generate higher radial force in the high-speed application can be used to develop a generalized test bench. The test bench can accommodate multiple types of bearings for testing.

REFERENCES/BIBLIOGRAPHY

- [1] R. S. Khurmi and J. K. Gupta, *Machine Design*, 2005th ed. Eurasia Publication House.
- [2] S. R. Pantula, “Automated Fault Diagnosis in Rotating Machinery.”
- [3] A. Klausen, R. W. Folger, K. G. Robbersmyr, and H. R. Karimi, “Accelerated Bearing Life-time Test Rig Development for Low Speed Data Acquisition,” *Model. Identif. Control Nor. Res. Bull.*, vol. 38, no. 3, pp. 143–156, 2017, doi: 10.4173/mic.2017.3.4.
- [4] W. Zhang, “A fault detection and diagnosis strategy for permanent magnet brushless DC motor,” p. 184.
- [5] “ISO 281:2007 Rolling bearings — Dynamic load ratings and rating life,” *ISO*. [Online]. Available:
<http://www.iso.org/cms/render/live/en/sites/isoorg/contents/data/standard/03/81/38102.html>.
- [6] “Instruments and parts from the industry partner.” .
- [7] “Difference between Radial and Thrust bearing,” 22-Feb-2019. [Online]. Available:
<https://www.bearing-manufacturers.com/difference-between-radial-and-thrust-bearing/>.
[Accessed: 10-Dec-2019].
- [8] D. E. R. Booser and M. M. Khonsari, “Grease life in ball bearings: The effect of temperatures,” p. 7.
- [9] “NSK_CAT_E728g Dynamic load rating, fatigue life, and static load rating by NSK.” .
- [10] J. S. Nam, H. E. Kim, and K. U. Kim, “A new accelerated zero-failure test model for rolling bearings under elevated temperature conditions,” *J. Mech. Sci. Technol.*, vol. 27, no. 6, pp. 1801–1807, Jun. 2013, doi: 10.1007/s12206-013-0431-1.
- [11] M. Khonsari and B. E.R., “Predicting Lube Life - Heat and Contaminants Are the Biggest Enemies of Bearing Grease and Oil.”
- [12] D. Kececioglu and J. A. Jacks, “The Arrhenius, Eyring, inverse power law and combination models in accelerated life testing,” *Reliab. Eng.*, vol. 8, no. 1, pp. 1–9, Jan. 1984, doi: 10.1016/0143-8174(84)90032-5.
- [13] J. Im, J. Park, and J. Hur, “Accelerated Life Test of Bearing under Electrical Stress,” p. 4.
- [14] M. Neale, *A guide to the condition monitoring of machinery*. HM Stationery Office, 1979.
- [15] J. H. Williams, N. Davis, and P. R. Drake, Eds., *Condition-based Maintenance and Machine Diagnostics*, 1994th ed. Springer Netherlands.
- [16] R. Randall, *Vibration-based Condition Monitoring: Industrial, Aerospace and Automotive Applications*. Wiley.
- [17] K. Worden and C. Farrar, *Structural Health Monitoring: A Machine Learning Perspective* . .

- [18]“ISO 281_2007 Bearing-Life Standard.” .
- [19]“Theory of Machine Book by R.S Khurmi and J.K Gupta.” .
- [20]“THK Caged Ball LM Guide.” .
- [21]“HIGH PRECISION BALL BEARINGS - IEC.” [Online]. Available:
<https://www.iecltd.co.uk/catalogues/grw/>. [Accessed: 19-Jan-2020].
- [22]“How does a Slip Ring Connector Work in the Electromechanical Industry?” [Online].
Available: <https://www.moflon.com/showen87.html>. [Accessed: 07-Nov-2019].
- [23]“Lessons In Electric Circuits -- Volume I (DC) - Chapter 8.” [Online]. Available:
https://www.ibiblio.org/kuphaldt/electricCircuits/DC/DC_8.html. [Accessed: 08-Nov-2019].
- [24]R. Randall, *Vibration-based Condition Monitoring: Industrial, Aerospace and Automotive Applications*. Wiley.
- [25]A. Zeiler, R. Faltermeier, I. Keck, A. Tomé, C. Puntonet, and E. Lang, “Empirical Mode Decomposition - an introduction,” presented at the Proceedings of the International Joint Conference on Neural Networks, 2010, pp. 1–8, doi: 10.1109/IJCNN.2010.5596829.

APPENDICES: A

MATLAB Code

```
Function: plot_scatter_fault_detection.m

%*****
%Fault Detection of the Bearings from Scatter Plot%
%*****

function [] = plot_scatter_fault_detection(PumpNo,ReadFile,
IMF_Rank)
%Taking input of PumpNo, ReadFile, IMF_Rank
% PumpNo      : Number of pump out of total tested pumps
% Read files: how many .CSV files to be taken for calculation
% IMF_Rank   : Represents the rank of IMF from EMD algorithm

% create directory from given files
dinfo = dir('*.*');

% Calculate the number of selected .CSV files
n = length (dinfo);

% Sorting file names in ascending order
FileNames = natsortfiles({dinfo.name}');

%*****Read the files and Calculating IMF values*****
%Files are selecting from the starting of test
for i = 1:ReadFile
    SpecificFileName = char(FileNames(i));
    FileRead = csvread(SpecificFileName,5,1);
    PumpRead1 = FileRead (:, PumpNo);

%Gnerating IMF with help of "emd" command
[imf1,residua,info] = emd(PumpRead1,'Interpolation','spline');
```

```

%Calculating Variance from the IMF
imf_variancel (i,:) = [(var(imf1(:,IMF_Rank)))]];
end

%*****Read the files and Calculating IMF values*****
%Files are selected from the end of the test
for j = n:-1:(n-ReadFile) %for k = ReadFile:-1:1
    SpecificFileName2 = char(FileNames(j));
    FileRead2 = csvread(SpecificFileName2,5,1);
    PumpRead2 = FileRead2 (:, PumpNo);

    %Gnerating IMF with help of "emd" command
    [imf2,residua,info] = emd(PumpRead2,'Interpolation','spline');

    %Calculating Variance from the IMF
    imf_variance2 (j,:) = [(var(imf2(:,IMF_Rank)))]];
end

%*****Scatter Plot*****

imf_variance3 = imf_variance2 ((n-ReadFile):n,1);
imf_variance_Y1 = imf_variancel;

%*****Plot for the Healthy Bearings*****
scatter (imf_variance_Y1, imf_variance_Y1,'g','filled')
hold on
imf_variance_Y2 = imf_variance3;

%*****Plot for the Faulty Bearings*****
scatter (imf_variance_Y2, imf_variance_Y2,'o','filled')
legend('Healthy Bearing','Faulty Bearing')

```

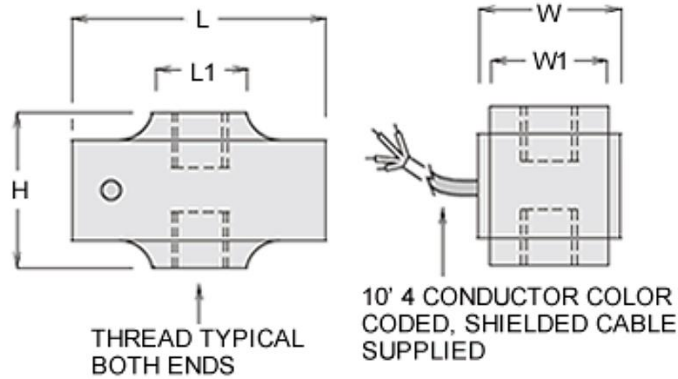

APPENDICES: B

Load Cell Data:

Manufacturer: Transducer Techniques

Model Code of load cell: MLP-10

Rated Output (R.O.): 2 mV/V nominal
 Nonlinearity: 0.1% of R.O.
 Hysteresis: 0.1% of R.O.
 Nonrepeatability: 0.05% of R.O.
 Zero Balance: 1.0% of R.O.
 Compensated Temp. Range: 60° to 160°F
 Safe Temp. Range: -65° to 200°F
 Temp. Effect on Output: 0.005% of Load/°F
 Temp. Effect on Zero: 0.005% of R.O./°F
 Terminal Resistance: 350 ohms nominal
 Excitation Voltage: 10 VDC
 Safe Overload: 150% of R.O.
 Calibration Included: Compression
 Optional Calibration: Tension



Model	Capacity (lb)	L	L1	W	W1	H	Thread d	Thread Depth (Inch)
		(Inch)						
MLP-10	10	1.50	0.6	0.54	0.37	0.75	10-32	0.2

VITA AUCTORIS

NAME: Nikunj Patel

PLACE OF BIRTH: Ahmedabad, India

YEAR OF BIRTH: 1991

EDUCATION: Gujarat Technological University, B.E., Ahmedabad,
India, 2013

University of Windsor, M.A.Sc., Windsor, ON, 2020